Chemistry Europe
European Chemical Societies Publishing

WILEY VCH

Excellence in Chemistry Research

Announcing our new flagship journal

- Gold Open Access
- Publishing charges waived
- Preprints welcome
- Edited by active scientists

Meet the Editors of *ChemistryEurope*

Luisa De Cola
Università degli Studi di Milano Statale, Italy

Ive Hermans
University of Wisconsin-Madison, USA

Ken Tanaka
Tokyo Institute of Technology, Japan

ChemCatChem

The European Society Journal for Catalysis

Chemistry Europe

European Chemical Societies Publishing

Supported by

GECATS GERMAN CATALYSIS SOCIETY

Accepted Article

Title: M-N-C Materials for Electrochemical Reduction Reactions: Recent Strategies for Improving Electrocatalytic Activity and Stability

Authors: Moisés A de Araújo, Andrey A Koverga, Alan M P Sakita, Felipe B Ometto, Letícia G da Trindade, and Edson A. Ticianelli

To be cited as: *ChemCatChem* **2023**, e202201594

Link to VoR: https://doi.org/10.1002/cctc.202201594

WILEY VCH

10.1002/cctc.202201594

WILEY-VCH

REVIEW

M-N-C Materials for Electrochemical Reduction Reactions: Recent Strategies for Improving Electrocatalytic Activity and Stability

Moisés A. de Araújo,*[a] Andrey A. Koverga,[a] Alan M. P. Sakita,[a] Felipe B. Ometto,[a] Letícia G. da Trindade,[a] and Edson A. Ticianelli,*[a]

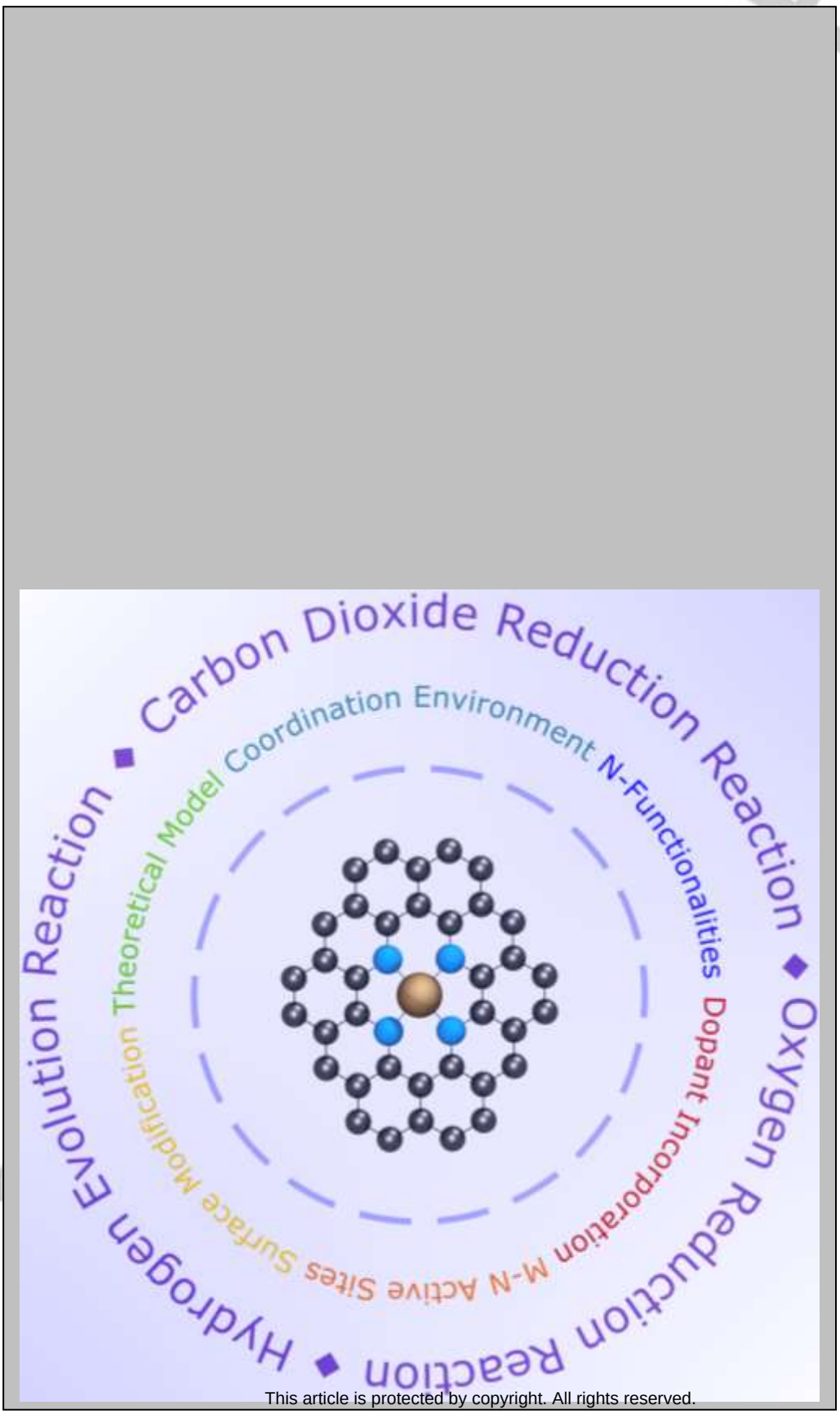

WILEY-VCH

REVIEW

[a] Dr. M. A. de Araújo, Dr. A. A. Koverga, Dr. A. M. P. Sakita, Dr. F. B. Ometto, Dr. L. G. da Trindade, Prof. Dr. E. A. Ticianelli
Instituto de Química de São Carlos
Universidade de São Paulo
Avenida Trabalhador Sancarlense, 400, postcode: 13566-590, São Carlos – São Paulo, Brazil
E-mail: edsont@iqsc.usp.br and moisesaaraujo@gmail.com

Abstract: Electrocatalytic reduction of small molecules such as dioxygen (O_2), carbon dioxide (CO_2), and water has driven conspicuous attention due to their technological importance and capability of tackling current environmental issues. So far, to drive such reactions, catalysts based on the platinum-group elements have displayed the best performance, however, the high-cost and scarcity of these elements hinder large-scale applications. Alternatively, earth-abundant M-N-C (M=Fe, Co, or Ni) materials have stood out as potential candidates because of their suitable electrocatalytic properties for the aforementioned reactions. In this way, the present review aims to provide a thorough account of the recently reported strategies to improve the electrocatalytic reduction of O_2, CO_2, and water on M-N-C catalysts. In order to have an in-depth understanding of these reactions, we will also discuss some of the latest theoretical studies based on computer modelling and simulation. Lastly, additional comments on future perspectives will be provided to guide new studies.

1. Introduction

The reduction of small molecules, e.g., water and oxygen gas (O_2) via the electrocatalytic hydrogen evolution reaction (HER) and oxygen reduction reaction (ORR), respectively, have been highly regarded for clean energy conversion in water electrolysers and fuel cells.[1] Comparing these reactions, the HER and ORR are closely intertwined for application in polymer-electrolyte-membrane fuel cell (PEMFC) in which hydrogen gas (H_2) is oxidised at the anode, whilst the ORR, i.e., the complementary reaction, takes place at the cathode.[2] One of the attractive features of the PEMFC is the absence of pollutant emissions, the emission product being only water, which can be converted again to H_2 and O_2 via, for example, (photo)electrochemical water splitting.[3,4] Additionally, the PEMFC is the most prominent candidate to be used as a power supply for electric vehicles, which stands advantageous to replace those using combustion engines and thus leading to contribute to reach the target of net-zero carbon emissions, including carbon dioxide (CO_2).[5] In this sense, the CO_2 reduction reaction (CO_2RR) may also play an important role in the mitigation of anthropogenic CO_2 emissions via converting CO_2 into value-added products.[6]

Despite the economic and environmental importance of the aforementioned reduction reactions, one drawback is their sluggish kinetics, which require the employment of appropriate catalysts to enhance their rates.[7,8] Pt features hitherto the best electrocatalytic activity for ORR and HER due to its moderate oxygen[9] and hydrogen binding energies (HBE),[10] respectively, as stated by Sabatier's principle.[11] However, the scarcity and high-cost of Pt hinder large-scale applicability.[12] For CO_2RR, Au and Ag are potential catalysts which can readily reduce CO_2-to-CO; nevertheless, also in this case, large-scale application is hampered by the scarcity and high-cost of these metals.[13]

Standing as alternative catalysts, M-N-C (metal coordinated to nitride-carbon materials) comprised of low-cost and earth-abundant transition metals (M=Fe, Co, or Ni) have shown promising electrocatalytic activity for ORR[9] as well as for HER[14] and CO_2RR.[14] The capability to catalyse these electrochemical reduction reactions enables to label the M-N-C as a multifunctional catalyst.

As a brief historical survey, the study of M-N-C catalysts was pioneered by Jasinski in 1964,[15] who found that nickel and cobalt phthalocyanines are active for the ORR. Later, heat-treated carbon-supported Fe-N_4 macrocycles (labelled as Fe-N-C) emerged as another type of potential ORR catalyst.[16] Since these initial studies, substantial improvements in catalytic activity and stability of M-N-C (M=Fe, Co, or Ni) have been achieved for ORR, CO_2RR, and HER over the years. Much of this advancement is owed to understanding the M-N-C molecular structure. So far, it is understood that M-N-C materials can be defined into three types of categories (see Figure 1). The first one comprises single-atom catalysts (SACs), which specifically contain atomically dispersed metal atoms. For such a structure, all the metal atoms are coordinated with nitrogen atoms in the carbon framework, meaning that there are no metal-metal bonds in the SAC structure.[17] It is also important to mention that M-N_x moieties are usually regarded as the active sites of the SAC-based M-N-C catalysts. The second category of M-N-C structure encompasses the carbon-supported metal nanoparticles encapsulated in N-doped carbon shells (labelled as M@NC). For this structure, the active site is considered to be the metal and nitrogen co-activated carbon sites. The third category is the combination of the two aforementioned structures (i.e., SACs&M@NC).[18] Herein, we will mainly review the studies of M-N-C materials featuring SAC structure for ORR, CO_2RR, and HER. This type of structure stands advantageous since it fully utilises metal atom contents, yet avoiding metal particle agglomerations stands as a major challenge to synthesise SAC-based M-N-C catalysts.[17]

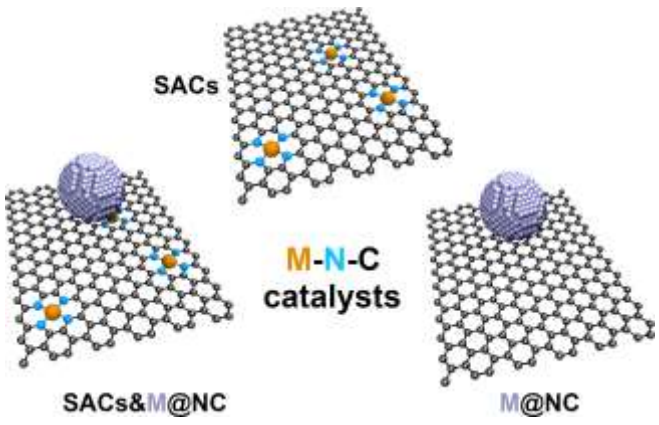

Figure 1. Schematic representation of the three types of structures for M-N-C materials.

Another important point concerns the characterisation to verify the formation of genuine SAC-based structure of M-N-C catalysts, which often requires advanced techniques, such as high-angle annular dark-field scanning transmission electron microscopy (HAADF-STEM), X-ray absorption spectroscopy (XAS), X-ray absorption near edge structure (XANES), extended X-ray absorption fine structure (EXAFS), and Mößbauer spectroscopy.[17,19,20] For example, HAADF images enable to verify atomic dispersion of metal sites which appears as bright dots due to the higher atomic number of the metal atom (higher capacity in scattering electrons) compared to the nitrogen and carbon elements.[17] In the case of XAS, both the oxidation state and chemical environment of the metal sites can be ascertained from the M K-edge XAS profiles.[19] Information about the oxidation state of metal sites can also be obtained by means of XANES spectra analysis.[19] Furthermore, the coordination environment of single sites in contrast to metal particles can be tracked by evidences present in the EXAFS spectra. In this way, the Fourier transform of the EXAFS (FT-EXAFS) signal in the Fe K-edge permits to distinguish of Fe-N or Fe-Fe bonds by calculated values of bond distances.[19] In the case of Mößbauer spectroscopy, it is employed in chemical characterisation as well as determination of oxidation state and coordination number of materials that usually contain iron.[21] For Fe-N-C catalysts, the significance of this technique stems from the fact that it can provide valuable information about the structure of iron active sites.[20]

Concerning synthesis methodology for SAC, many preparation methods have been developed for the sake of obtaining highly active SAC-based M-N-C materials. In this context, since the study developed by Gupta et al.[22] in 1989, much progress has been achieved in the preparation of M-N-C catalysts involving the heat-treatment step. Currently, as illustrated in Figure 2, the most employed methodology involves pyrolysis of mixtures containing a transition metal salt precursor, and nitrogen and carbon sources.[23,24] Single precursor reagents containing all the elements (i.e., transition metal, nitrogen, and carbon) have also been employed, for which metal-organic frameworks (MOFs) are often used.[25] In all cases, the pyrolysis step is carried out at high temperatures (~600-1200 °C), under N_2 or Ar atmosphere.[26] This pyrolysis approach may lead to the formation of agglomerated metallic particles or metal-carbide particles, together with SAC embedded in the N-doped carbon.[27] This heterogeneity of M-N-C catalysts may have a deleterious effect on the overall electrocatalytic performance as well as difficulty in identifying and quantifying the genuine active sites. To prevent/minimise heterogeneity occurrence, one common approach after the pyrolysis process is to acid washing the pyrolyzed material for removal of aggregated metal-based particles to ultimately obtain a real SAC catalyst. This approach may be followed by a second pyrolysis procedure under N_2, Ar, or NH_3 atmosphere, which usually aims to improve the electrical conductivity of M-N-C catalysts and to restore the graphitic and M-N_x structure.[18]

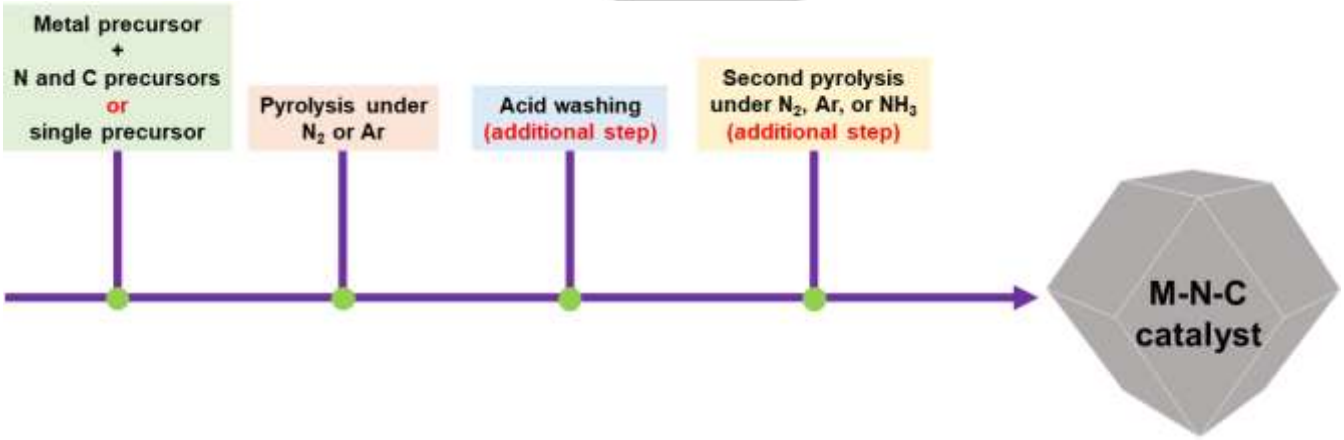

Figure 2. Schematic representation of the typical synthesis route for M-N-C catalysts.

The presented topics, namely the advanced characterisation approach and synthesis methodology, have hugely contributed to the design of SAC-based materials with improved electrocatalytic performance. Nevertheless, M-N-C materials have not yet delivered high enough electrocatalytic activity and durability to drive ORR, HER, and CO_2RR at large-scale applications. Additionally, it is still challenging the obtainment of an M-N-C catalyst having high-density of structurally well-defined active sites uniformly distributed in the N-C network. Although more studies are required to overcome these challenges, much has been advanced over the past few years in terms of synthesis optimisation, active site understanding, and improvement of stability and electrocatalytic performance of these materials.

In light of these advancements, the aim of this article is to review the strategies recently developed to improve electrocatalytic performance and stability of M-N-C (M=Fe, Co, or Ni) materials for the ORR, CO_2RR, and HER. Moreover, this review also aims to provide a description of the latest theoretical studies that allowed further understanding of the M-N-C (M=Fe, Co, or Ni) materials as catalysts for the aforementioned reduction reactions. This review was organised into three sections, each one dealing with a particular electrochemical reduction reaction, namely ORR, CO_2RR, and HER. In each case, we present the reported results of experimental and theoretical studies, for providing an understanding of the electrocatalytic activity and stability of M-N-C (M=Fe, Co, or Ni) materials for the given electrochemical reduction reaction.

Moisés A. de Araújo received his BSc degree in Chemistry (2013) and MSc degree in Chemistry (2015) from the *Universidade Federal do Ceará* and *Universidade Federal de São Carlos* (UFSCar), Brazil, respectively. He obtained his PhD degree in Science (2020) from the UFSCar, Brazil. Currently, de Araújo is a postdoctoral fellow at the *Universidade de São Paulo,* Brazil, working on the obtainment of earth-abundant chalcogenide-based semiconductor films for (photo)electrochemical H_2 generation and CO_2RR under the supervision of Prof. Edson A. Ticianelli. de Araújo's research interests span application of nanostructured semiconductor thin films for photoelectrochemical and photovoltaic cells systems.

Andrey A. Koverga received his PhD from the Medellín branch of *Universidad Nacional de Colombia*, Colombia, in 2020. After completing one-year postdoctoral fellowship at the *Instituto Tecnológico de Aeronáutica*, Brazil, he joined Edson Ticianelli's electrochemical group at the *Universidade de São Paulo*, Brazil. His major research interest is theoretical modelling and description of novel materials in energy storage/conversion applications.

Alan M. P. Sakita completed his doctorate at the *Universidade Estadual Paulista "Júlio de Mesquita Filho"*, Brazil, where he studied the electrodeposition of iron metal group in deep eutectic solvents for electrocatalysis purposes. After receiving his PhD, he started postdoctoral research on carbon-based materials for energy storage devices at the *Universidade Federal de Minas Gerais*, Brazil. Currently, he is a postdoctoral fellow at the *Universidade de São Paulo*, Brazil, working on the electrochemical reduction of carbon dioxide employing carbon-supported catalysts under Prof. Ticianelli's supervision.

Felipe B. Ometto holds a BSc (2011) and PhD (2019) degree in Chemistry from the *Universidade Estadual Paulista "Júlio de Mesquita Filho"*, Brazil. Currently, he is a postdoctoral fellow at the *Universidade de São Paulo*, Brazil. He has experience in chemistry, with an emphasis on Electrochemistry, working mainly with fuel cells for electrical energy conversion and electrolysers for dihydrogen production.

Letícia G. da Trindade received her PhD degree from the *Universidade Federal do Rio Grande do Sul* (UFRGS), Brazil, in 2015. After that, she worked as a research fellow at the *Universidade Federal de São Carlos*, Brazil, UFRGS, Brazil, and the *Universidade Estadual Paulista "Júlio de Mesquita Filho"*, Brazil. da Trindade is currently a postdoctoral fellow at the *Universidade de São Paulo*, Brazil, working at the synthesis, modification, and characterisation of proton conductive polymers for fuel cells under the supervision of Prof. Edson A. Ticianelli. Her major research interests are in conductive polymers and nanomaterials for energy conversion applications.

Edson A. Ticianelli has been a professor at the *Universidade de São Paulo* (USP), Brazil, since 1977, and has been appointed *livre-docente* (1992) and full professor (2003) positions also from the USP. He holds an MSc degree (1980) and a PhD degree (1985) in Physical Chemistry, both from the USP. Between 1986 and 1998, he carried out several placements in institutions from the United States, namely Los Alamos National Laboratory and Brookhaven National Laboratory. Ticianelli's research topics include the development of catalysts for fuel cells, electrolysers and CO_2RR, the preparation and modelling of gas diffusion electrodes, and the study of ORR.

2. M-N-C (M=Fe, Co, or Ni) electrocatalysts for the ORR

This section will be fully addressed via reviewing the latest studies, and for such, we have carefully selected studies that encompassed an in-depth understanding of the M-N-C electrocatalytic nature (e.g., active site characteristics) for ORR. Additionally, we have focused our attention on the studies that provided substantial advancement of ORR performance and durability on M-N-C that are comparable or even superior to those of the Pt/C benchmark material.[28]

As for many other catalysts, it has been accepted that the ORR mechanism on M-N-C materials may involve four-electron or two-electron processes, in which the adsorption of O_2 ($O_{2(ads)}$) is the first step; after this, there are two possible pathways to proceed with the reduction reaction: O_2 dissociation or hydrogenation, the former being more unlikely to occur than the latter.[29] The hydrogenation of $O_{2(ads)}$ results in the formation of adsorbed OOH species, that may be further reduced involving or not the breaking of the O-O bond, depending on the nature of the catalyst and/or its corresponding adsorption energy for OOH. As seen reaction schemes of Figure 3, this is a crucial step because it determines the subsequent reaction mechanism type, i.e., four-electron or two-electron ORR process.

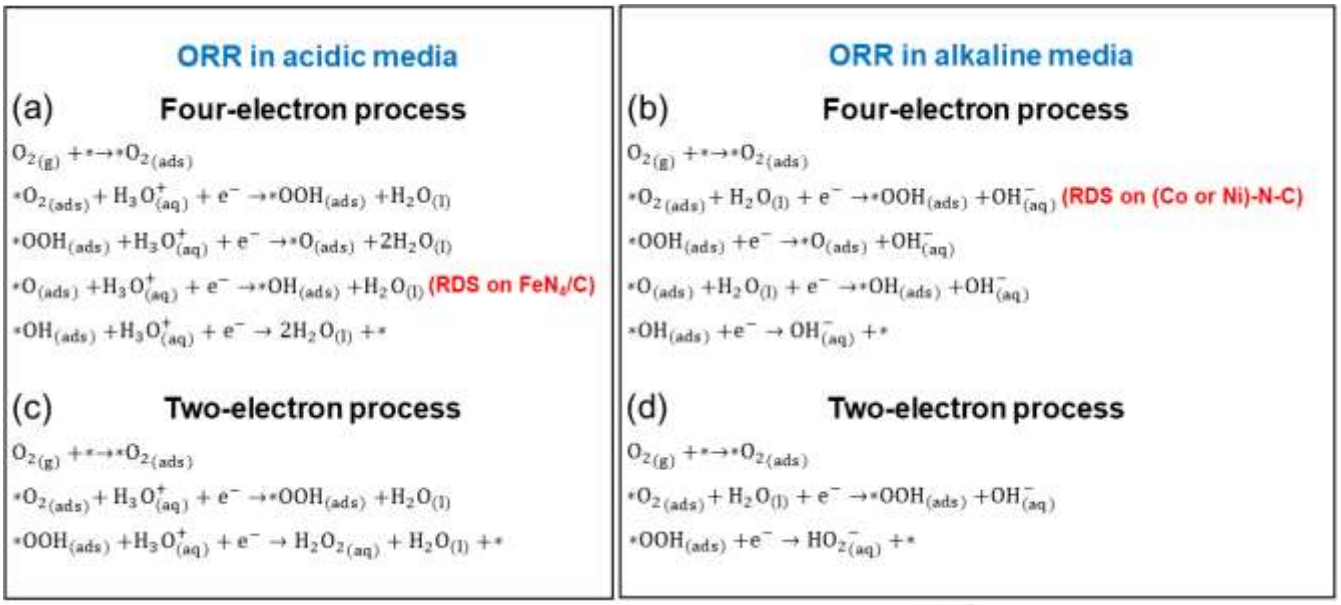

Figure 3. Probable four-electron reaction pathway for the ORR on (a) FeN_4/C in acidic[29] and (b) M-N-C (M=Fe, Co, or Ni) in alkaline media.[30] Probable two-electron reaction pathway for the ORR in (c) acidic and (d) alkaline media.[31] RDS is the rate-determining step and the asterisk (*) denotes the active site.

In terms of product generation, the four- and two-electron ORR processes lead to the formation of H_2O (in acidic or OH^- in alkaline electrolytes) and H_2O_2 (in acidic or HO_2^- in alkaline electrolytes), respectively.[31] The generated H_2O_2 or HO_2^- may undergo further reduction via another two-electron process to produce water in acidic media and OH^- in alkaline media. The occurrence of two subsequent two-electron processes is classified as indirect four-electron ORR.[32] For fuel cell applications, it is preferable to have the direct four-electron ORR, because it provides higher energy conversion efficiency. Also, avoiding the formation of H_2O_2/HO_2^- subproducts is crucial, since radical species generated by such products can attack fuel cells' components, compromising the durability of the system.[18] In this way, it is utterly important to have M-N-C catalysts highly selective for the four-electron ORR mechanism.

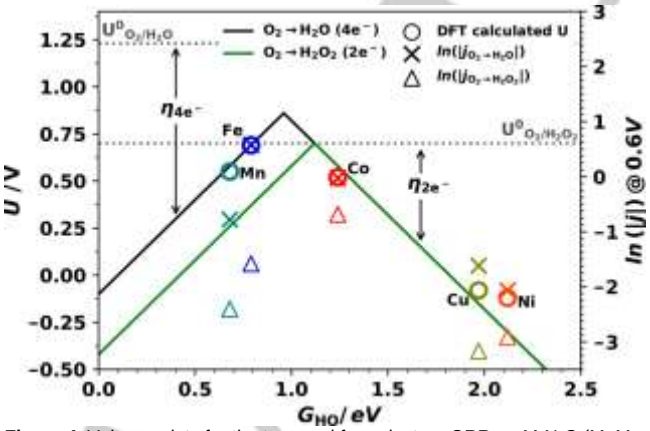

Figure 4. Volcano plots for the two- and four-electron ORR on M-N-C (M=Mn, Fe, Co, Ni, or Cu) materials. Reprinted with permission from Ref.[33] Copyright 2019, American Chemical Society.

Considering the M-N-C (M=Fe, Co, or Ni) materials, it has been shown that Fe-N-C features a predominant four-electron process (Figure 4).[33] Additionally, Fe-N-C material is regarded as the most promising electrocatalyst due to its high activity towards ORR.[34] In this sense, we shall focus on mainly reviewing this material for ORR, first in acidic media and then in alkaline electrolytes.

Fe metal centre – acidic electrolytes

Considering first the preparation methods, many approaches have been considered, for example that involved Fe-N-C material obtained by one-step pyrolysis at temperatures near 1000 ℃, and employing a zeolitic imidazolate framework (ZIF) as a source of nitrogen and carbon, combined with an iron precursor reagent.[35,36] Biomass has also been considered as a source of nitrogen and carbon since it is an economical and abundant natural resource.[37] Additionally, biomass activation with phosphoric acidic was found to lead to a higher carbon corrosion resistance to the Fe-N-C catalysts, which is a major deleterious effect causing loss of active Fe-N_x sites.[38]

Efforts have been extensively made to modulate the coordination environment of the active sites in Fe-N-C materials with SAC-based structures. Prior to delving into this, it is important to note that there are several mainstream hypotheses about the nature of these active sites. As summarised in Figure 5, the active sites may include N-C groups, which have poor ORR electrocatalytic performance, as well as oxidised iron ($FeO_x(C_y)$) and iron particles embedded in N-doped carbon (Fe@N-C), being both prone to undergo degradation.[39] Other proposed SAC-type active sites may include Fe-N_x and Fe_2N_x, and these two are highly regarded since they possess high stability and ORR electrocatalytic performance compared to the other mentioned active sites.[39]

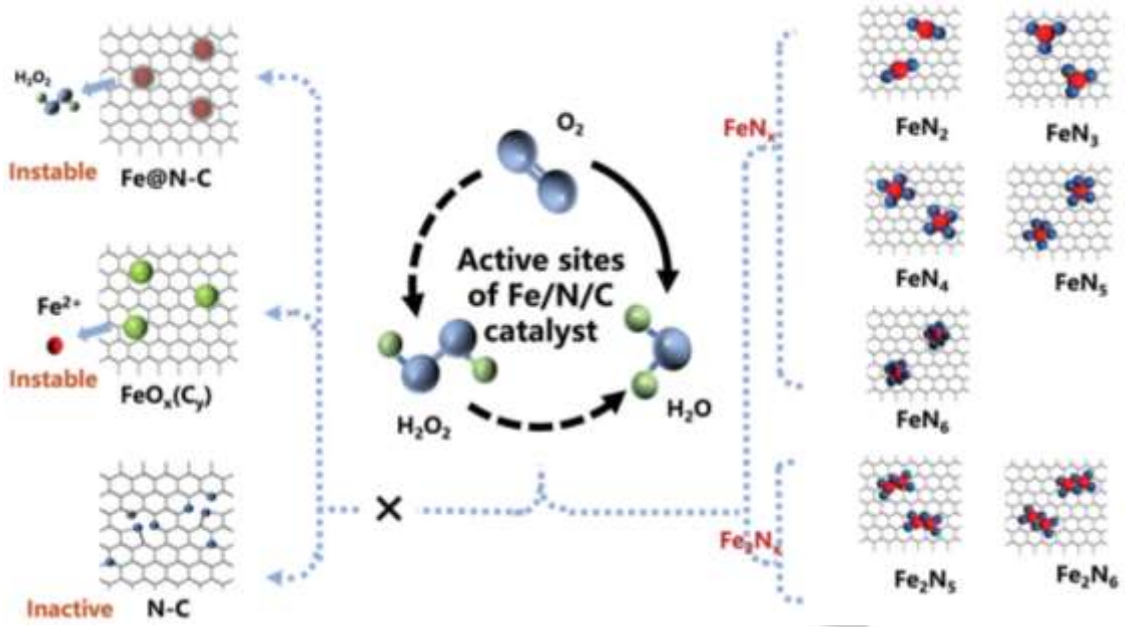

Figure 5. Possible active sites in Fe-N-C catalysts for ORR. Reproduced from Ref.[39] under the terms of the Creative Commons Attribution CC BY License, https://creativecommons.org/licenses/by/4.0/.

As also shown in Figure 5, the Fe-N_x sites may be present in at least five coordination modes, such as Fe-N_2, Fe-N_3, Fe-N_4, Fe-N_5, and Fe-N_6.[39] Among these modes, a study demonstrated that Fe-N_5 moieties present increased ORR activity and stability (for up to 11.1 h), which is comparable to the benchmark Pt/C catalyst in acidic media.[40] In another study,[41] it was shown that the coordination number of the Fe-N_x (x=1, 3, 4) sites in Fe-N-C materials can be tailored via the pyrolysis temperature, so that at 300 ℃ favour the formation of Fe-N, whereas temperatures of 500 and 1000 ℃ enable the formation of Fe-N_3 and Fe-N_4, respectively. The authors also systematically evaluated the ORR performance of these catalysts and the results suggested that Fe-N_4 presents higher ORR activity compared to the Fe-N_x (x=1, 3). The effect of pyrolysis temperature above 1000 ℃ has also been assessed and it was shown that pyrolysis at 1100-1300 ℃ can serve the purpose of improving the stability of Fe-N-C materials in PEMFC.[42] This has been concluded on the basis of ^{57}Fe Mößbauer analyses, which showed that materials treated at temperatures in the range of (1100-1300 ℃) can change the Fe-N-C coordination structure, from less stable D1 (O-FeN_4C_{12}, featuring N-pyrrolic coordinated to Fe) to a more electrocatalytic and stable D2 (FeN_4C_{10}, having N-pyridinic coordinated to Fe) (see Figure 6a).

As reported in another study, the coordination structure of the Fe-N_x active sites in the Fe-N-C catalyst was also evaluated during ORR via in situ analyses of XAS measurements. Based on analyses of XANES and EXAFS, see Figure 6b-e, it was noted that the increase of potential (from 0.1 to 0.9 V vs. reversible hydrogen electrode (RHE)) may have led to different morphological changes in the Fe-N_4 sites (i.e., Fe moving towards or away from the N_4-plane) in the potential range of ORR (Figure 6f). Moreover, it was shown that the ORR activity is essentially governed by the dynamics of the Fe^{2+}/Fe^{3+} redox transition, rather than the static structure of the bare sites.[43]

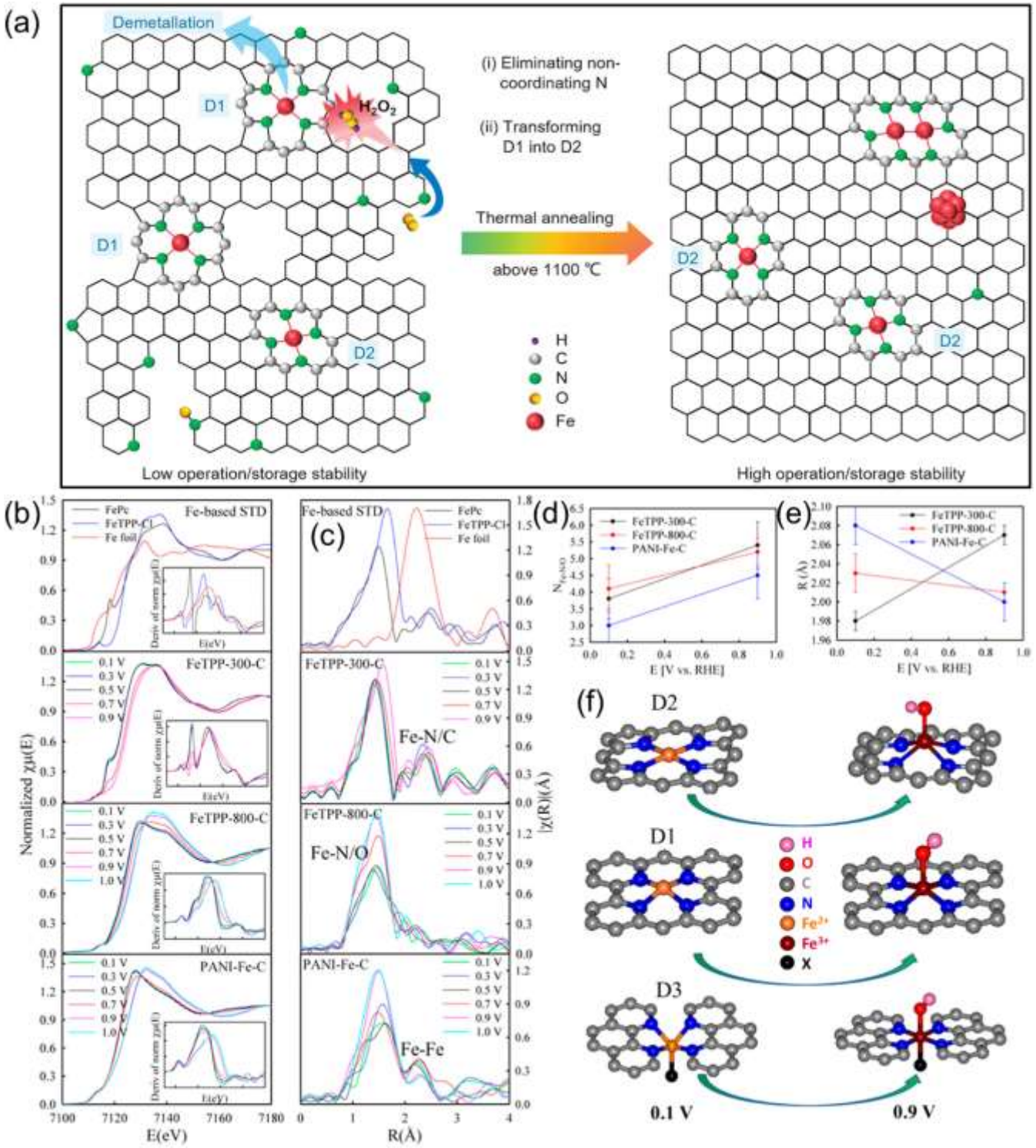

Figure 6. (a) Schematic illustration of microstructure evolution at pyrolysis temperature above 1100 ℃ for ORR stability improvement of Fe-N-C catalyst. Reproduced (adapted) with permission.[42] Copyright 2022, Wiley. (b) XANES spectra at the Fe K-edge with concomitant first derivatives (insets) and (c) FT-EXAFS as a function of the applied potential for Fe-N-C catalysts. (d) coordination numbers and (e) bond distances as a function of the applied potential for Fe-N-C catalysts. (f) Schematic illustration of Fe-N switching behaviour designated by three structural models ($Fe\text{-}N_4\text{-}C_x$) labelled as D_2, D_1, and D_3, respectively, with/without axially bond $O(H)_{(ads)}$. The atom labelled as X represents the fifth ligand with its identity unknown. Reprinted (adapted) with permission from Ref.[43] Copyright 2015, American Chemical Society.

Besides these presented studies about iron's coordination environment engineering, other strategies that enable the improvement of ORR performance and stability involve the modulation of the nitrogen functionality. As summarised in Figure

7a, the nitrogen functionality can be classified as pyridinic-N, pyrrolic-N, and graphitic-N. A recent study demonstrated that SAC-type Fe-N-C materials featuring Fe coordinated to pyridinic-N enabled substantial improvement of ORR stability compared to that of Pt/C in acidic medium.[44] Moreover, theoretical analyses demonstrated that pyridinic-N has stronger binding energy (BE) with Fe single atoms compared to pyrrolic-N, meaning that high content of pyridinic-N can better stabilise the Fe-N-C catalysts. Nitrogen functionality also plays a role in the selectivity of the ORR. In this context, it has been demonstrated that Fe-N-C catalysts having pyridinic Fe-N_4 present better selectivity for four-electron ORR in acidic medium compared to the Fe-N-C catalyst coordinated with pyrrolic-N.[45] Another recent strategy that permitted the enhancement of stability and ORR electrocatalytic performance is the introduction of dopants, such as sulphur.[36,46] In this regard, a stepwise synthesis strategy (Figure 7b) has enabled to obtain Fe-N-C materials featuring sulphur doping of a rich carbon mesoporous structure, obtained by pyrolysis at temperatures in the range of 600-900 ℃ (Figure 7c-d). The catalyst pyrolyzed at 800 ℃ delivered a remarkable activity and impressive stability for the ORR compared to that of the Pt/C catalyst in acidic media.[47]

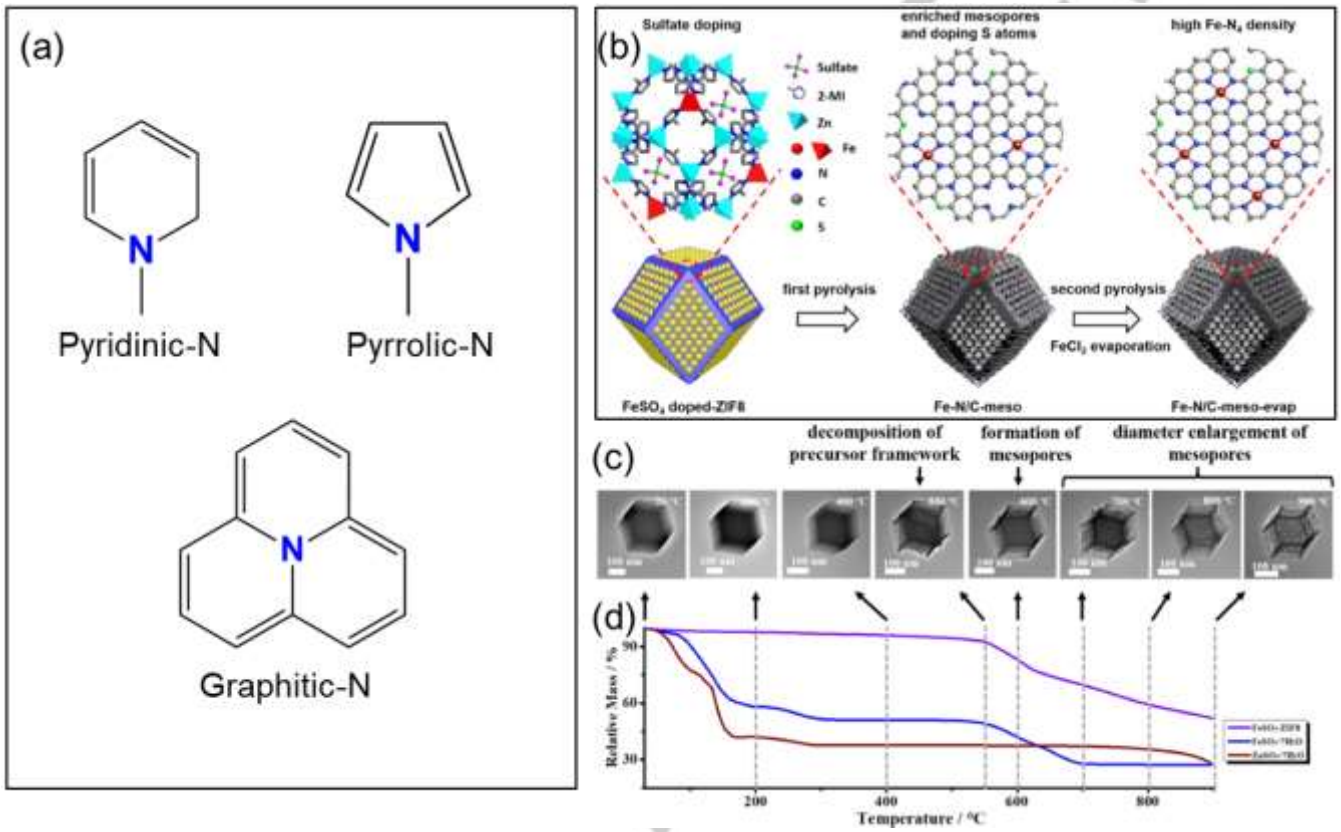

Figure 7. (a) Types of nitrogen functionality. (b) Stepwise synthesis procedure of Fe-N-C catalyst. (c) Transmission electron microscopy images and (d) thermogravimetric analysis curves for the formation mechanism of rich mesoporous structures of Fe-N-C catalyst. Reprinted (adapted) from Ref.[47], Copyright 2021, with permission from Elsevier.

Another recent study has provided an additional understanding of the nature of the active sites in Fe-N-C catalysts.[48] In this way, based on analyses of ^{57}Fe Mößbauer spectra and density functional theory (DFT) calculations, the presence of Fe-N_x moieties as Fe(III)N_4C_{12} in high-spin state and Fe(II)N_4C_{10} in the low and medium spin state have been identified. It was also reported that the former is present as surface-exposed sites, whereas the latter is either at bulk sites (inaccessible for O_2) or as surface sites (however leading to weaker O_2 bindings compared to Fe(III)N_4C_{12} site).[48] In addition to active site identification, another study has reported a methodology to accurately quantify the active site density and catalytic turnover frequency on Fe-N-C catalyst. For such, the low-temperature (−80 ℃) CO pulse chemisorption technique was employed, followed by temperature-programmed CO desorption.[27] This methodology is particularly important since it allows meaningful comparisons between catalysts, and could favour a more rational development of materials with enhanced electrocatalytic properties.

Despite these substantial advances toward the synthesis of materials with improved electrocatalytic activity, the stability of Fe-N-C material is still a major issue, particularly in acidic media. So far, the stability of Fe-N-C material most often spans only dozens of hours under acidic media, which is considerably inferior compared to the several thousands of hours required for commercial applications.[49] To meet commercial the stability target, it is pivotal to have a clear understanding of the degradation mechanisms of these materials, as it could pave the way for designing more durable catalysts in acidic media. However, the degradation mechanism of Fe-N-C in the course of ORR in acidic media is not yet entirely well understood. Currently, as summarised in Figure 8, it is understood that the main factors for the Fe-N-C degradation in acidic media are linked to (i) carbon matrix corrosion; (ii) Fe demetallation; (iii) protonation of N-

groups; (iv) microporous flooding; and (v) conductance loss.[39] Among these possible degradation factors, carbon corrosion and Fe demetallation are considered the major causes that compromise catalysts' lifetime. Briefly, carbon corrosion refers to the chemical reaction of the carbon matrix of Fe-N-C with O_2, H_2O_2, or other reactive oxygen species (i.e., a product of ORR side reaction) to produce CO or CO_2.[39] The demetallation process is problematic because the dissolution of iron ions from the catalyst in the acidic medium can catalyse the conversion of H_2O_2 (a by-product of ORR) into radicals via the Fenton reaction (cf. Equations (1) and (2)).[39]

$$Fe^{2+}_{(aq)} + H_2O_{2(aq)} \rightarrow Fe^{3+}_{(aq)} + HO^{\bullet}_{(aq)} + OH^{-}_{(aq)} \quad (1)$$

$$Fe^{3+}_{(aq)} + H_2O_{2(aq)} + H_2O_{(l)} \rightarrow Fe^{2+}_{(aq)} + HOO^{\bullet}_{(aq)} + H_3O^{+}_{(aq)} \quad (2)$$

The formation of radical species, such as hydroxyl (HO•) and hydroperoxyl (HOO•), stands as a major issue as these radicals could cause degradation of the carbon matrix and Fe-N-C's active sites, which may progressively escalate the dementalization process and thus the Fenton reaction.[39]

In view of the recurrent demetallation issue, it has been recently questioned whether the absence of iron sites in the Fe-N-C catalyst could affect the ORR performance in acidic media. Aiming to address this fundamental question, Kong et al.[50] demonstrated that N-doped carbon materials having trace amounts of iron (0-0.08 wt%) delivered excellent ORR activity and durability comparable to those of the Pt/C catalyst in both alkaline and acidic media without the major contribution of the iron sites. The authors claimed that the presence of noncovalently bonded N-deficient/N-rich interlayers served as active sites for the ORR. Despite this advancement, the question concerning the role of iron sites in Fe-N-C is still open, pending a full understanding of the active sites' nature in Fe-N-C or N-doped carbon materials. In another study that also aimed to minimise the degradation process, it was shown that the SAC iron sites, namely FeN_xC_y, seem to be more resistant to demetallization compared to the particulate iron Fe@N-C sites.[51] For the sake of minimising operando demetallation of Fe-N-C material in acidic media, other recent studies have shown that the employment of bimetallic M-N-C catalysts, such as (Fe, Co)-N-C[52] and (Fe, Ni)-N-C,[53] can potentially increase catalyst's stability in acidic media. Additionally, the improved stability of bimetallic M-N-C systems may be due to the dual-metal sites that facilitate the dissociation of O-O bond in HOO*, suppressing the H_2O_2 production and consequently the degradation process.[49]

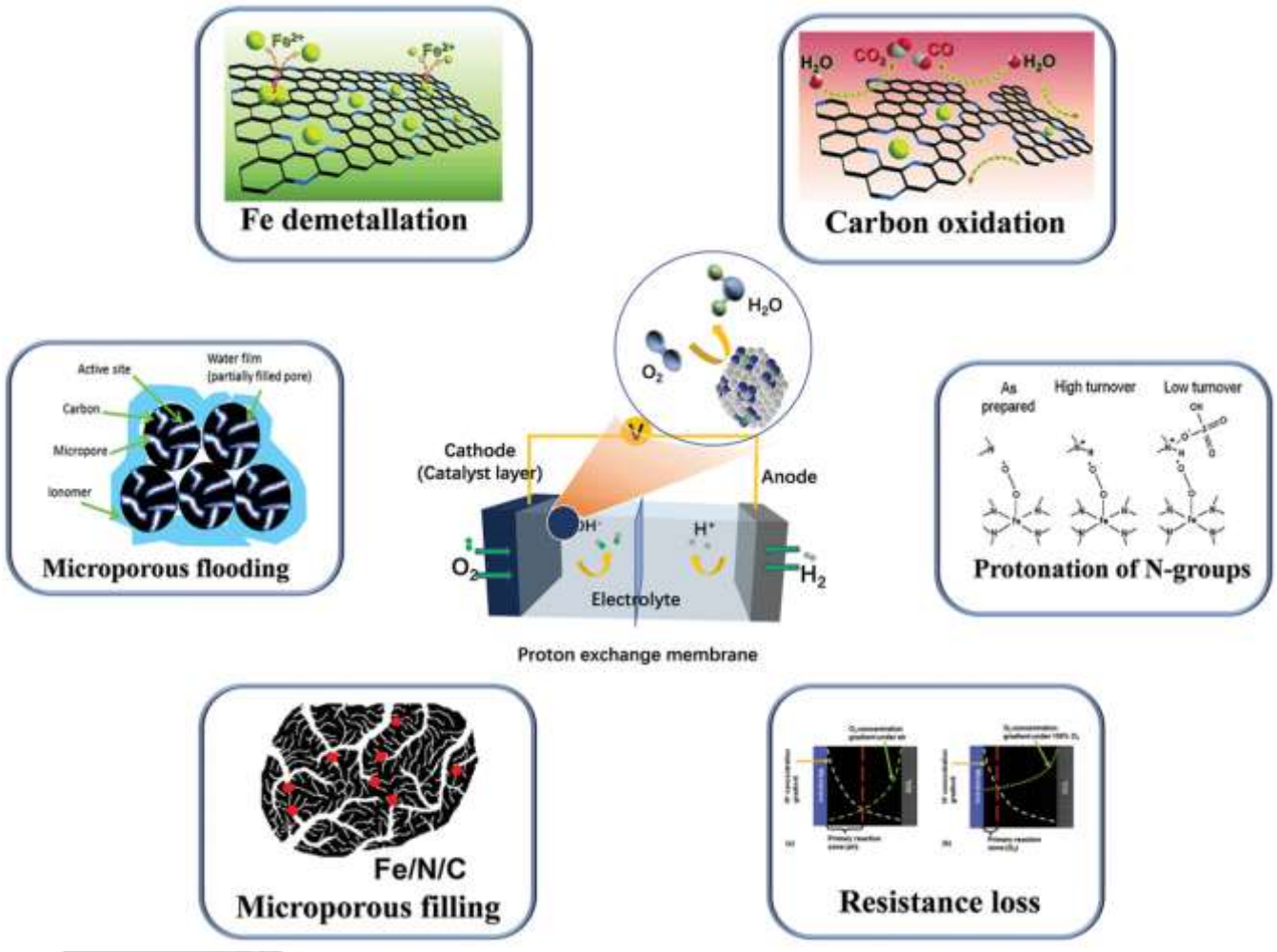

Figure 8. Probable degradation mechanisms for Fe-N-C catalyst. Reproduced from Ref.[39] under the terms of the Creative Commons Attribution CC BY License, https://creativecommons.org/licenses/by/4.0/.

Fe metal centre – alkaline electrolytes

The stability and electrocatalytic activity of Fe-N-C catalysts present a better scenario in alkaline, rather than acidic media. The increase in stability is mostly due to the Fenton reaction being hindered since the dissolved iron ions are precipitated into iron oxohydroxides and hydroxides. Additionally, alkaline media lead to an acceleration of H_2O_2 self-decomposition into O_2 and H_2O as well as a decrease of $HO^{\bullet}$ oxidation potential (e.g., the oxidation potential of the redox couple $HO^{\bullet}/H_2O$ is 2.59 V vs. standard hydrogen electrode (SHE) at pH 0 and 1.64 V vs. SHE at pH 14).[54]

Recent studies of the activity and stability of Fe-N-C material as catalysts for the ORR in alkaline media were conducted by Sgarbi et al.[55], by assessing the electrochemical transformation of Fe-N-C catalyst into iron oxide and its effect on the ORR electrocatalysis. Also, the authors were able to provide a comprehensive understanding of the iron dissolution/iron oxide reprecipitation mechanism occurring along an accelerated stress test (AST). The results suggested a possible synergic effect between the redeposited iron oxide particles and untransformed SAC Fe-N_xC_y moieties, that provided stability for the catalyst along the AST. Another way to improve chemical stability, electron mobility, mass-transfer rates, and consequently ORR activity on Fe-N-C catalyst is via the employment of a carbon-based three-dimensional interpenetrating network structure, which enables the presence of increased at-edge Fe-N_x moieties located at the boundaries and interfaces of this kind of structure.[56]

It has also been found that modifying Fe-N-C structures by the introduction of dopants, such as sulphur[57–59] and phosphorus,[60] can lead to improvement of stability and electrocatalytic activity of ORR in alkaline media. It is proposed that dopants introduce two possible changes in the SAC configurations: (i) sulphur atom might replace one of the nitrogen atoms in the Fe-N_4 site thus bonding directly to the metal centre (forming $FeSN_3$);[57] or (ii) sulphur atom might be bonded to carbon (i.e., thiophenic-S) neighbouring the Fe-N_4 site (forming FeN_4SC).[58] For phosphorus dopants, analyses of EXAFS spectra indicated that the phosphorus atom might be bonded to the Fe-N_4 site in a penta-coordination structure (i.e., FeN_4P).[60] In general, these dopants can improve the stability and electrocatalytic performance of Fe-N-C catalysts, since they favour the adsorption of key ORR intermediates.[57,58,60]

Improvement of the activity towards ORR in alkaline media can also be achieved by using Fe-N-C catalysts prepared using highly aligned hierarchical porous carbon structures, combined with a sulphur dopant.[61],[62] Two factors have been assigned for explaining the improved activity provided by this approach: (i) the presence of densely distributed active sites provided by the high-specific-surface-area of the hierarchical porous structures;[61,63,64] and (ii) the optimisation of the Fe-N_x centres promoted by sulphur dopant, that induces a charge enrichment of Fe-N leading to optimal O_2 bindings that minimises the reaction barrier and favour ORR kinetics. In another illustrative study, Rauf et al.[65] designed a Fe-N-C catalyst with Fe-N_x and pyridinic-N embedded in a carbon-based mesoporous matrix (Figure 9a). As shown in Figure 9g-l, Fe-N-C catalyst presented enhanced ORR performance as well as long-term stability compared to the Pt/C catalyst. The improved stability was associated with the low H_2O_2 yield (≤1.5%), see Figure 9j, whilst the enhanced ORR activity was related to the high content of pyridinic-N forming the SAC Fe-N_x active sites (Figure 9b-f). In another study, the performance and stability of the Fe-N-C catalyst were evaluated when this material was integrated into the cathode of an H_2/O_2 anion-exchange membrane fuel cell (AEMFC). It was shown that this material delivered good performance and stability in the AEMFC, similar to a system containing a Pt/C cathode.[66]

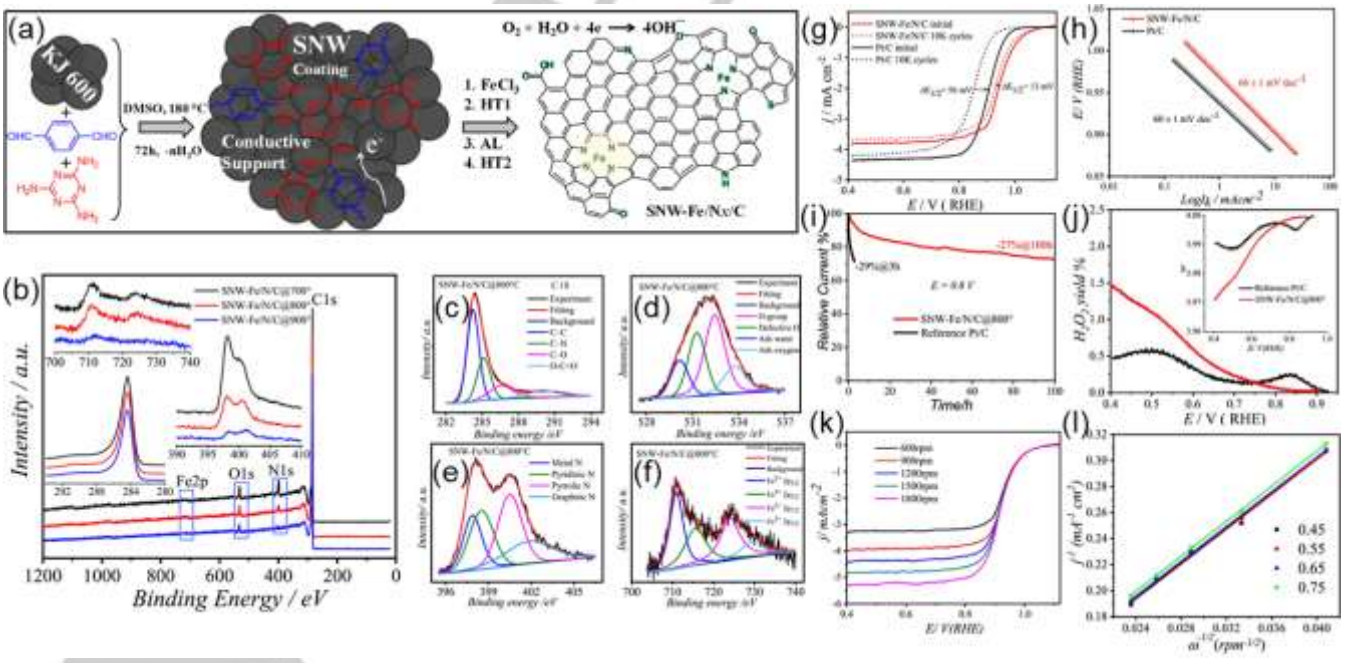

Figure 9. (a) Schematic representation for synthesis preparation of Fe-N-C catalysts. X-ray photoelectron spectroscopy spectra of (b) survey and high-resolution for (c) C 1s, (d) O 1s, (e) N 1s, and (f) Fe 2p of Fe-N-C catalysts. (g) ORR polarization curves before and after 10,000 cycles, and (h) Tafel plots for Fe-N-C and Pt/C catalysts in O_2-saturated 0.1 mol L^{-1} NaOH solution. (i) Chronoamperometric curves at 0.8 V vs. RHE for Fe-N-C and Pt/C materials under the rotating rate of

900 rpm and in O_2-saturated 0.1 mol L^{-1} NaOH solution. (j) H_2O_2 yield and electron transfer number during ORR on Fe-N-C and Pt/C catalysts. (k) ORR curves for Fe-N-C catalyst obtained under different rotation rates, and (l) the corresponding Koutecký-Levich plots at different potentials. Reprinted (adapted) from Ref.[65], Copyright 2021, with permission from Elsevier.

The Fe demetallation process of Fe-N-C material may also take place in alkaline media. Employing a gas diffusion electrode (GDE) in a half-cell setup with liquid electrolyte, coupled to an online inductively coupled plasma mass spectrometry system, it was shown that the demetallation process can occur under conditions close to those in fuel cells operating conditions, i.e., at current densities (*j*) up to −125 mA cm^{-2} and with a porous Fe-N-C catalyst layer.[67] It is proposed that a way to minimise Fe demetallation in alkaline media is via the generation of carbon vacancies in the SAC-based Fe-N-C material. From DFT calculations, it was shown that these vacancies can reduce the adsorption free energy of HO*, consequently hampering the Fe demetallation process.[68] Another strategy to improve the stability and electrocatalytic activity of ORR on Fe-N-C in alkaline media is via increasing the density of Fe-N_x active sites.[69–71] In this context, Wang et al.[69] employed a facile benzoate-assisted self-template strategy to obtain an SAC-based Fe-N-C catalyst featuring a high density of easily accessible active sites. Compared to the state-of-the-art Pt/C catalyst, this material delivered excellent ORR performance in alkaline solution and good stability with 90% of the initial activity retained after 90 h of a continuous running experiment. It is worth mentioning that the use of sodium benzoate during the synthesis was essential to stabilise iron ions in the Fe-N-C structure, which favours the minimisation of ORR electrocatalytic loss arising from Fe demetallation. The benzoate-based chemical reagent also contributed to improving the ORR performance via the increase in the content of SAC-based structures that enlarge the surface-active area. Another important observation is that, together with the increase of Fe-N_x active sites density, there is an increase of metal atom agglomerations (i.e., metal not coordinated with nitrogen atoms), which could be less active for ORR. As reported recently, this issue can be circumvented by adjusting the solvent during Fe-N-C synthesis.[70] For example, comparing methanol and water/methanol, the employment of the aqueous medium enabled to obtain a high density of Fe-N_x sites and hindered the formation of iron-based nanoparticles during the pyrolysis process.

Metal centres other than Fe

Studies in both acid and alkaline electrolytes denote that degradation of Fe-N-C structures remains a challenge, mostly because of the Fe demetallation process that could trigger the Fenton reaction under H_2O_2 presence in acidic media.[72] Thereby, M-N-C materials containing alternative metals that do not catalyse the Fenton reaction have been under consideration. Presently, Co is regarded as an alternative metal for M-N-C materials since this element is less catalytic compared to Fe to start off the Fenton reaction.[73] Nevertheless, ORR activity on Co-N-C material is generally lower than on Fe-N-C.[35,74] Another drawback is that Co-N-C catalysts have exhibited higher H_2O_2 yield (>5%) compared to Fe-N-C catalysts.[73] The stability of Co-N-C materials stands as another critical bottleneck that requires fundamental studies about their degradation mechanism. Several hypotheses have been proposed and one of the possible degradation pathways is the dissolution of Co ions from the Co-N_x active sites during the ORR in acidic media.[73] Recent studies employing hierarchical porous structures for providing high-specific-surface-area have demonstrated to improve the performance and stability of Co-N-C, either in acidic or alkaline electrolytes.[75,76] Another approach to improve electrocatalytic activity and stability is via immobilisation of Co-N_4 moieties in ZIF-8 micropores, which consists of doping ZIF-8 with Co using Co-Zn ion exchange followed by pyrolysis. Such an approach enabled a significant increase in the density of Co-N_x active sites in the SAC-based Co-N-C structure. As a result, high catalytic activity for ORR was achieved, comparable to Fe-N-C in acidic medium, but with superior durability.[72]

Besides cobalt, nickel is another alternative substitute for iron in M-N-C catalysts since it also has a poorer activity for the Fenton reaction.[77] Compared to Fe-N-C and Co-N-C materials, Ni-N-C has been less studied for ORR as its ORR electrocatalytic activity is deemed unsatisfactory both in acidic and alkaline media, which may be due to the Ni site in the Ni-N_x weakly binds with the ORR intermediates.[77,78] Another important aspect to bear in mind is that similar to Co-N-C material, Ni-N-C also features ORR selectivity towards H_2O_2 production. Albeit more studies are required, it has been suggested that H_2O_2 production on Ni-N-C materials may take place at graphene edge defects and in nonmetal nitrogen sites in the N-C matrix.[33] A theoretical study predicted that one way to favour the four-electron ORR activity is via coordinating boron to the NiN_4-C system. Among different combinations of boron substitution in the NiN_4-C system, NiN_2B_2-C featured suitable adsorption energy for the ORR intermediates that favoured the improvement of four-electron catalytic activity.[77] Another recent study demonstrated that the employment of substrates with a high volume of mesopores enabled to obtain Ni-N-C catalysts featuring high-specific-surface-area. This enlarged surface area favoured a great exposure of Ni-N_x active sites which consequently facilitated the ORR on the Ni-N-C material catalyst in alkaline medium.[79]

DFT studies

Until this point, we have mainly focused on reviewing experimental studies of ORR on M-N-C catalysts, but theoretical studies based on chiefly the DFT approach have also enabled advancement in the understanding of many aspects of different reduction reactions. In this regard, we shall present the following concepts assessed theoretically for ORR, which is the main reaction regarded for M-N-C systems. The d-band centre[80] and electronegativity of the nearest atoms[81] are usually considered as descriptors of the ORR activity of Fe-N_4 active centres (ACs). However, these intrinsic characteristics do not explain the orientation dependence and differences in ORR activity at the same FeN_4 site on different carbon supports. In this regard, a fundamental study of single-atom Fe-N-C[82] demonstrated that magnetic moments on Fe and O_2, and the d-band centre gap of spin states correlate significantly better than the mentioned descriptors for ORR activity. Interestingly, in the same study, a poor correlation was mentioned between the adsorption energy of O_2 and ORR activity at the Fe-N_4, even though O_2 adsorption is the first step of ORR on M-N-C materials. On the other hand, the O_2 adsorption stability on the MN_4/C surface was considered a prerequisite for the material to be able to catalyse the ORR.[29] In

another study, atomic oxygen BE was used to estimate the ORR activity of square-planar and square-pyramid ACs.[83] Specifically, it is believed that a too weak O binding catalyst usually has difficulty in the formation of *OOH intermediate on the surface, while too strong O binding may lead to slow rate-determining removal of *OH intermediate. Therefore, the question of a reliable ORR activity descriptor of M-N-C materials remains open and requires further theoretical and experimental investigation.

It is also important to mention that the stability of various ORR intermediates on a catalyst's surface may have an impact on its catalytic activity. Adsorbate-substrate interaction, in its turn, is largely defined by the fundamental properties of both adsorbate and surface. Therefore, the electronic properties and geometry of the ACs play an important role, impacting the catalytic activity of M-N-C towards ORR. A study by Zheng et al.[83] revealed that most square-planar ACs, MN_xC_{4-x} (M=Fe, Co, or Ni), strongly adsorb the ORR intermediates, resulting in their lower catalytic activity. Additionally, Fe atoms in the Fe-N_4 centres were found to be positively charged while the N atoms were negatively charged, which is beneficial for O_2 adsorption.[29] The total net charge on the AC can also have an effect on the RDS: for Co and Ni, the reduction of adsorbed O_2 to peroxide radicals is the RDS (Figure 3b), whereas for, Fe, which has the lowest positive charge compared to the other metals, the RDS corresponds to the process of charging and desorption of the hydroxide ions.[30]

Final remarks on ORR

To summarise this topic, several remarks can be made. First, it is noted that the electrolyte pH plays a pivotal role in the stability and ORR electrocatalytic performance on M-N-C (M=Fe, Co, or Ni) materials, and alkaline media has been found to be the suitable condition to date. It should also be mentioned that the most successful strategies to improve ORR performance and stability of M-N-C (M=Fe, Co, or Ni) materials in alkaline media involve: using a substrate with hierarchical porous structures, forming high-density M-N_x active sites, introducing defects (e.g., carbon vacancies formation), and adding dopants. These strategies enabled electrocatalytic improvement due to the increased M-N_x active sites exposure, enhanced electrolyte penetration, stabilisation of metal centre in M-N-C structure, and moderate adsorption strength of intermediates. Regarding the stability of M-N-C materials, among the reviewed M-N-C (M=Fe, Co, or Ni) materials, Fe-N-C and Co-N-C catalysts have stood out so far as the most durable materials and with the highest electrocatalytic activity for ORR. Additionally, it has been shown that these materials are stable for up to hundreds of hours under alkaline conditions. Despite the tremendous advancements, the stability times are not satisfactory compared to the thousands of hours target established by the US Department of Energy.[84] To fulfil such a long-term stability target, further studies are required to help design more suitable Fe-N-C and Co-N-C catalysts.

3. M-N-C (M=Fe, Co, or Ni) catalysts for the CO_2RR

Prior to delving into the description of the latest studies about CO_2RR on M-N-C (M=Fe, Co, or Ni) materials, it is worth mentioning that we have devoted our attention to the studies that featured electrocatalytic performance and stability, which are promising compared to benchmarking flat catalysts.[85] It should be noted that different from the previous section that was indicated the electrolyte pH, herein, however, such a distinction will not be made (unless specified) since the experiments of CO_2RR are usually carried out in CO_2-saturated bicarbonate-based electrolytes at pH of ca. 7.0.

Considering initially the CO_2RR mechanism, a typical mechanism of CO_2RR comprises a four-step process (Figure 10a) producing CO as the main product. Despite its apparent simplicity, this mechanism allows the understanding of the catalytic trends observed for MN_4C_{10} clusters,[86] estimating the impact of theoretical model parameters on predictions of Fe-N-C poisoning,[87] and defining a potential RDS for CO_2RR on the M-N_x (x=1-4) ACs.[88] For systems, where further CO hydrogenation is possible, a more complex mechanism is often required in addition to the initial four-step process, as it has been observed for M-N-C systems, where M=Fe, Ni, Cu, Zn, Ru, Rh, Pd, Ag, Cd, Os, Ir, Pt, or Au.[89] Also, the mechanism for CH_4 generation has been proposed (Figure 10b), with the step formation of CH_2OH* being thermodynamically the most favourable. However, this mechanism was only possible on (Ir or Rh)-N-C, since on other systems, such as Ni-N-C, further CO hydrogenation was hindered by weak CO BE and its fast desorption from the surface.

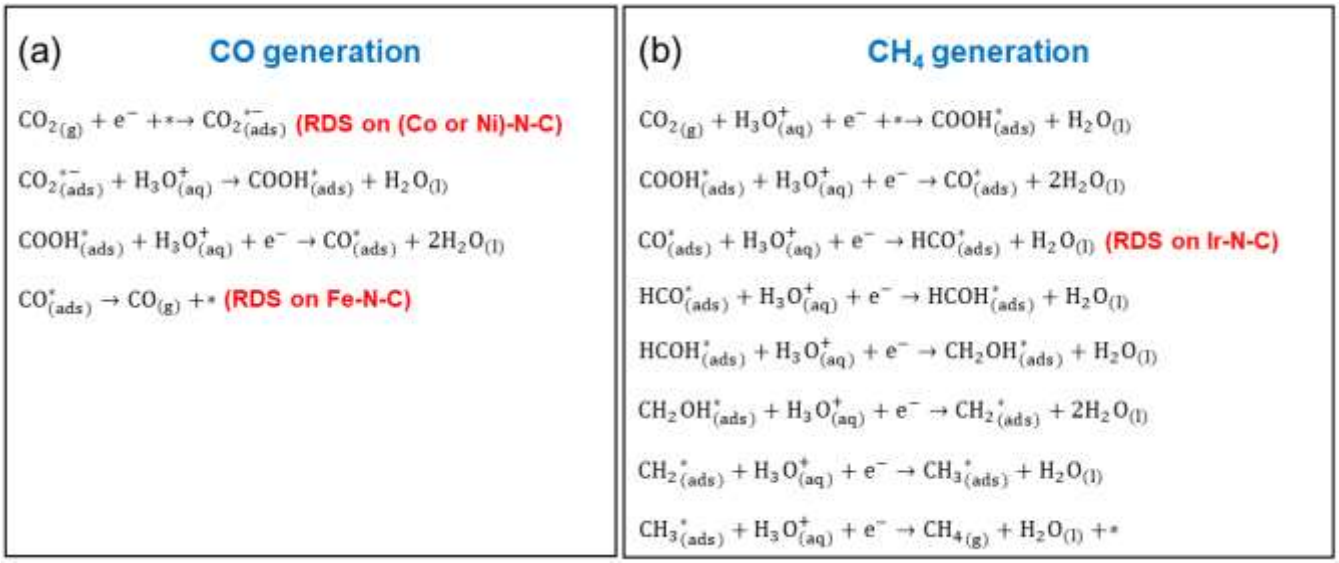

Figure 10. Probable reaction pathways of CO_2RR to (a) CO and (b) CH_4 on M-N-C (M=Fe, Co, or Ni)[86] and (Ir or Rh)-N-C materials,[89] respectively.

In this way, an important general aspect is that most M-N-C catalysts display high selectivity for CO_2-to-CO conversion due to their moderate BE of the adsorbed reaction intermediate species.[90] Additionally, it is understood that the CO_2RR selectivity highly depends upon the nature of the metal centre in M-N-C catalysts. Theoretical analyses assessed the product selectivity of $M-N_4$ sites in M-N-C with different metal centres, namely Mn, Fe, Co, Ni, or Cu, for CO_2RR and it was observed the following increasing trend of CO production: Co-N-C ≈ Cu-N-C < Mn-N-C < Fe-N-C < Ni-N-C. Overall, Ni-N-C and Fe-N-C catalysts are the most promising candidates for CO generation since they offer a better trade-off between CO selectivity and bias input. In other words, Ni-N-C features the highest CO selectivity at high overpotentials, whereas Fe-N-C provides relatively high CO selectivity at low overpotentials. It is also interesting to mention that Ni-N-C possesses weak binding to H* leading to an unfavourable HER, which often competes with the CO_2RR at high overpotentials.[91]

Aiming to improve selective CO generation on M-N-C catalysts, recent studies have focused on controlling the coordination environment of the metal centre.[92,93] As summarised in Figure 11, different coordination configurations can be found for the $Ni-N_x$ active sites in Ni-N-C. In this context, a recent theoretical study has scrutinised several NiN_xC_{4-x} (x=1-4) sites, and it was found that pyrrolic-type $Ni-N_4$ moiety (i.e., β-NiN_4) has higher selective CO_2-to-CO conversion in contrast to the HER.[94] Based on free energy diagram analyses, it was also further learnt that CO_2-to-CO conversion on β-NiN_4 can be favoured, since this moiety type features a moderate energy barrier for the intermediate species of the CO_2RR and a high barrier for H* formation (Volmer reaction). Another study has shown that the employment of a pyrolysis temperature of 1000 ℃ favoured the formation of Ni-N-C catalyst featuring coordination numbers of two N and two C atoms (i.e., $Ni-N_2C_2$). Compared to the other N/C coordination numbers, the $Ni-N_2C_2$ catalyst delivered the highest CO faradaic efficiency (FE_{CO}) of 98.7% at −0.7 V vs. RHE. In addition to the coordination environment effect, another important aspect to mention is the interference on the CO_2RR performance caused by extra uncoordinated N atoms coexisting with $M-N_x$ sites in the M-N-C catalysts. Regarding this, Wang et al.[95] greatly improved CO_2RR on Co-N-C with diminished uncoordinated N species. This catalyst delivered an outstanding FE_{CO} of 99.4% at −0.60 V vs. RHE.

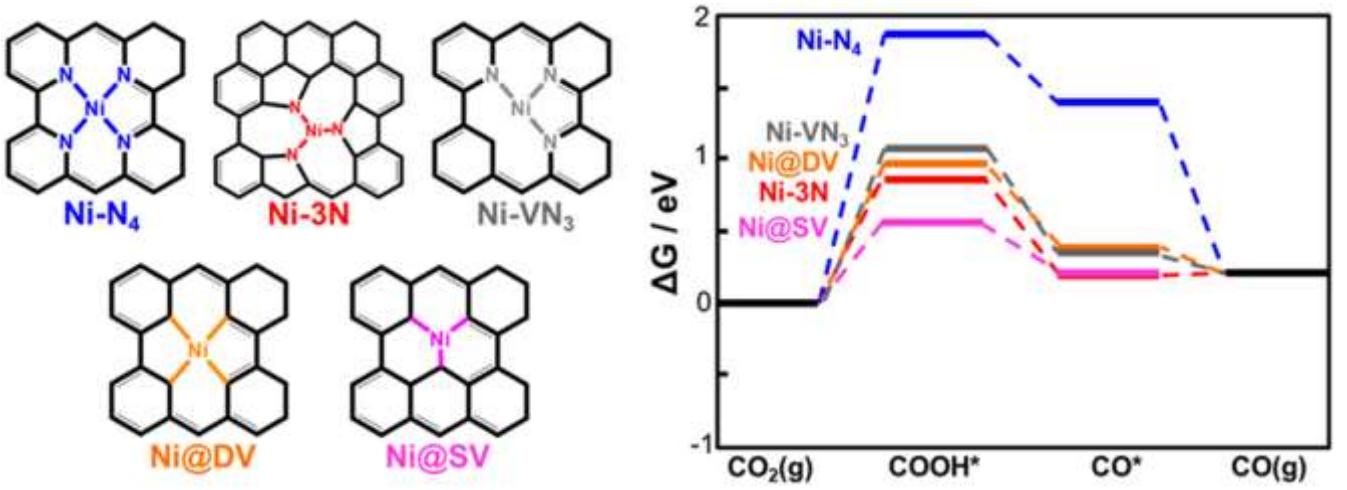

Figure 11. Schematic representation of the different Ni-N_x active sites and CO_2RR free energy diagram over these active sites. Reprinted (adapted) with permission from Ref.[96] Copyright 2019, American Chemical Society.

In an effort to further improve the CO_2-to-CO conversion on M-N-C catalysts, recent studies have also been dedicated to modifying the active sites (i.e., M-N_x) with dopants, such as sulphur.[97,98] In this context, Lu et al.[99] obtained sulphur-doped Ni-N-C catalyst via ion-adsorption and pyrolysis treatment. Compared to S-free Ni-N-C material, the Ni-NS-C catalyst displayed outstanding FE_{CO} of nearly 100% and stability with negligible activity decay after 19 h. Based on DFT calculations, the high activity and selectivity toward CO formation were assigned to the synergetic effect of the S and Ni-N_x moieties. Still, in connection with the dopants approach, it was reported that bonding phosphorus dopant to the metal centre (Fe-N_x) had enabled improvement of the CO_2-to-CO reaction.[100]

Other illustrative studies have described Ni-N-C as a superior catalyst for syngas generation (mixture of H_2 and CO) due to its higher j/FE_{CO} ratio.[101] Unlike Ni-N-C catalyst, Fe-N-C material often displays lower j for CO_2RR, but it shows high selectivity for CO generation. Another way to enhance the M-N-C catalysts' performance is the confinement of ionic liquids (ILs) into their porous structure. The employment of ultrasonication-centrifugation methodology for the nanoconfinement of ILs into porous Ni-N-C proved to increase the j (about 2.7-fold) and the FE_{CO} (99.6%), compared to the bare catalyst (Figure 12a-b).[102] This superb activity was assigned to the IL role as CO_2 concentrator, and/or co-catalyst, and/or HER suppressor. Furthermore, it has also been shown that during the CO_2RR the imidazolium-based ILs, namely $[Bmim]^+$, can stabilise the intermediate CO_2^{*-} via the formation of [Bmim]-CO_2 complex (Figure 12c), that increases the local CO_2 concentration near the catalyst surface, and lowers the energy barrier for CO_2-to-CO conversion.[102] Besides the ILs approach, a strategy based on proton capture is another way to improve selective CO generation on Ni-N-C materials containing Ni nanoparticles adjacent to the Ni-N_x active sites. Joint experimental and theoretical analyses demonstrated that the Ni nanoparticles accelerate the adsorbed hydrogen generation to be transferred to the adjacent Ni-N_x active sites for improving the protonation of the intermediate and the overall CO_2-to-CO conversion.[103] In addition to the CO_2-to-CO conversion on M-N-C materials, the formation of methane (CH_4) has also been shown to be possible on Fe-N-C catalysts.[104] It has also been shown that the CH_4 production rate on Fe-N-C catalyst can be improved at low electrolyte pH (i.e., pH 2), nevertheless, the CH_4 faradaic efficiency was low due to the predominance of the HER at such a pH condition.[105] For CO_2-to-CO conversion, it has been demonstrated that the electrolyte pH does not affect the CO production rate on Fe-N-C catalysts, thus suggesting that alkaline media could be an ideal condition to favour CO selectivity over H_2 generation. However, this electrolyte condition leads to the conversion of CO_2 into carbonic acid, which results in lowering the electrolyte pH. The occurrence of this phenomenon constraints the pH range of CO_2-saturated solution to work with CO_2RR, i.e., it is limited to the acidic and neutral conditions.[96]

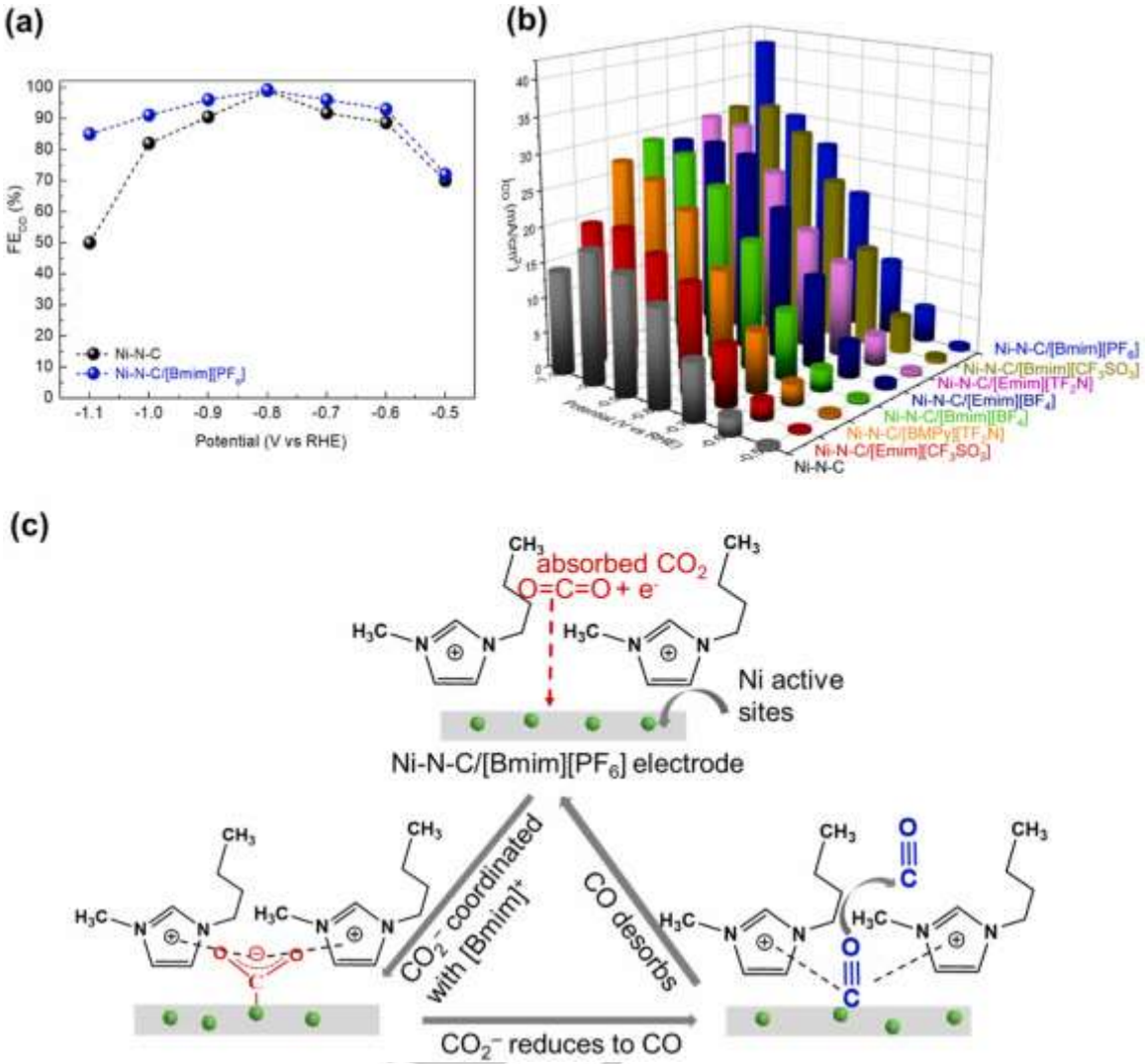

Figure 12. (a) FE_{CO} for Ni-N-C catalyst and Ni-N-C/[Bmim][PF_6] composite catalyst. (b) j_{CO} values for Ni-N-C catalyst and Ni-N-C/[ILs] composite catalysts. (c) CO_2RR mechanism on Ni-N-C/[Bmim][PF_6] composite catalyst. Reprinted from Ref.[102], Copyright 2021, with permission from Elsevier.

Besides catalytic activity, the long-term stability of M-N-C materials for industrial CO_2 electrolysers (up to 50,000 h)[85] is another important feature to be considered, yet it still lacks an in-depth fundamental understanding of M-N-C materials' degradation mechanism under harsh operation conditions of CO_2RR. Nevertheless, DFT-based screening analyses have demonstrated that the M-N-C (M=Fe, Co, or Ni) materials are among the most structurally stable and experimentally operable (see Figure 13a).[106] In a recent study, it has been achieved good stability over 50 h for CO_2-to-CO conversion on an SAC-based Ni-N-C catalyst featuring a pyrrole-type Ni-N_4 structure. Additionally, a slight attenuation in both *j* and FE_{CO} was observed, which resulted in ca. −3.6 mA cm^{-2} and 80% at −0.7 V vs. RHE, respectively.[107] Despite these results being promising, the *j* value was not high enough to meet the target for industrial levels (i.e., >200 mA cm^{-2}).[85] As recently reported, one way to improve both *j* and stability time is via using Ni-single atom self-supported on porous carbon fibre membrane (NiSA/PCFM) catalysts, which was prepared by an electrospinning method (cf. Figure 13b).[108] Such a membrane catalyst employed in a GDE cell setup delivered outstanding CO partial current density (j_{CO}) of −308.4 mA cm^{-2} as well as FE_{CO} of 88% at −1.0 V vs. RHE, and stability time up to 120 h. It is also interesting to mention that running the CO_2RR experiments in a GDE device enabled substantial improvement of j_{CO} and stability time compared to the conventional H-type cell (see Figure 13c-e). The effect of flow cell setup on the CO_2RR performance was also demonstrated by Wang et al.[109] Employing a SAC-based Ni-N-C coupled with nanostructured zirconium oxide in such a cell resulted in a *j* of −200 mA cm^{-2}, which is suitable for commercial application, as well as a high FE_{CO} of 96.8% at −1.58 V vs. RHE. In another study, Wang and co-workers[110] have recently demonstrated that SAC-based Co-N-C has better stability than SAC-based Ni-N-C and this may be due to its good resistance to demetallation. Besides Ni-N-C and Co-N-C materials, combined experimental and theoretical studies have demonstrated that the introduction of axial chlorine (Cl) in the Fe-N_4 active sites can improve the selectivity of CO_2RR over HER as well as the catalyst stability. The FeN_4ClNC exhibited a maximum FE_{CO} of 90.5% and j_{CO} of −9.78 mA cm^{-2} at −0.6 V vs. RHE as well as stability time over 18 h in a conventional H-cell. Based on DFT calculations, the presence of axial Cl coordination on single Fe of FeN_4ClNC

catalyst favoured CO* desorption and hindered H* adsorption, thus enabling improvement of activity and selectivity for CO_2-to-CO conversion.[111] Another study has demonstrated that SAC-based Fe-N-C featuring uniformly dispersed Fe-N_4 sites with adjacent Fe_3C nanoparticles enabled achieving good stability (up to 30 h) and high FE_{CO} of 94.6% at −0.5 V vs. RHE. Based on additional characterisation analyses and theoretical calculations, it is proposed that the improved CO_2-to-CO conversion may have been due to the presence of Fe_3C nanoparticles that strengthen the adsorption of CO_2 on the isolated Fe-N_4 sites to ultimately accelerate the formation of COOH*.[112]

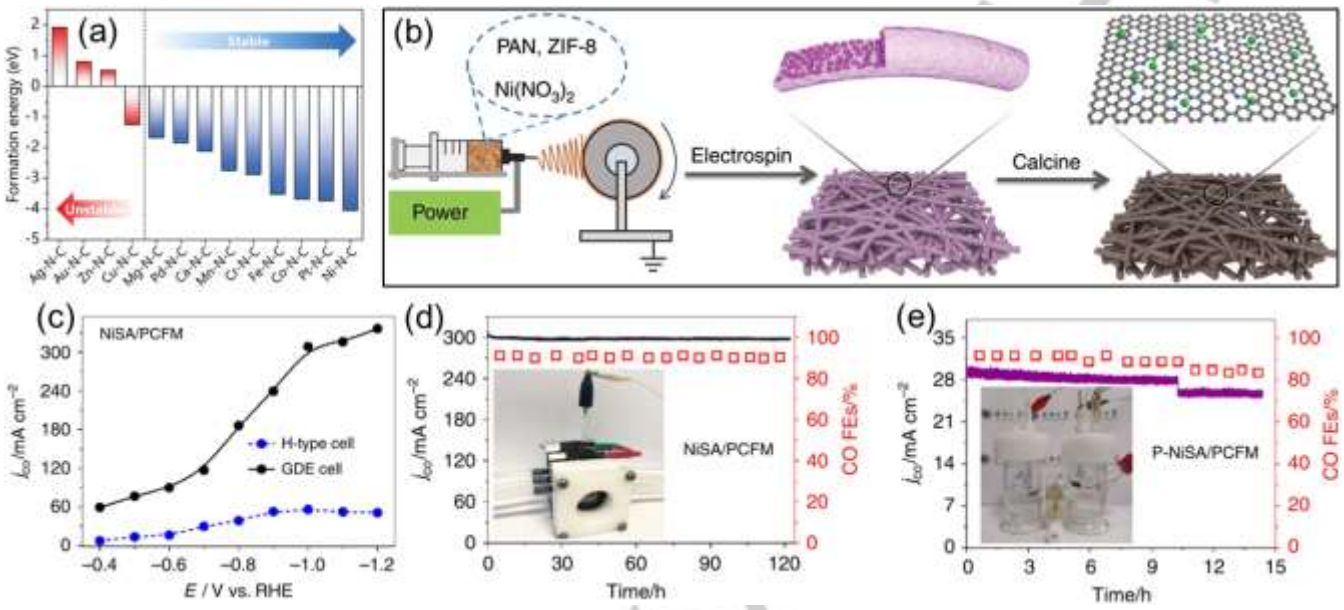

Figure 13. (a) Structure stability of M-N-C (M=Ag, Au, Zn, Cu, Mg, Pd, Ca, Mn, Cr, Fe, Co, Pt, and Ni) materials based on the formation energy. Reproduced (adapted) with permission.[106] Copyright 2021, Wiley. (b) Representation of synthesis approach of NiSA/PCFM catalyst. (c) j_{CO} values for NiSA/PCFM catalyst in different cells set-up. Stability tests in (d) GDE cell and (e) H-type cell at −1.0 V vs. RHE. Reproduced from Ref.[108] under the terms of the Creative Commons Attribution CC BY License, https://creativecommons.org/licenses/by/4.0/.

DFT studies

In addition to the mainly considered experimental studies, the theoretical investigation also greatly contributed to the understanding of the electrocatalytic behaviour of M-N-C materials for CO_2RR. According to DFT studies, the BE of the COOH* intermediate generated during CO_2RR (Figure 10) is one of the most common choices as a CO_2RR activity descriptor. The HBE (a well-known descriptor for catalytic activity towards HER) has also been used to understand the competition between the CO_2RR and HER on metals and M-N-C catalysts.[113] Moreover, it has been shown that one of the key advantages of the M-N-C family compared to metallic surfaces, is that M-N-C materials do not have hollow sites – preferable location for H adsorption. Lately, COOH and CO BEs have been employed as descriptors for CO generation over M-N_x ACs,[88] and Ni-N_4 was found to be the site with the most optimal properties for CO production. Fe- and Ni-based M-N-C were also predicted to be optimal catalysts for CO_2RR to CO, as indicated by the combination of activity (CO BE) and selectivity descriptors (difference between the BE for CO_2^{*-} and HBE).[86] Another study explained good CO selectivity on Ni-N-C by the low HBE and weak CO binding, which facilitated CO removal from its surface.[89] This, however, made Ni-N-C systems unfit for CO conversion to hydrocarbons. In agreement, the ability of the AC in M-N-C to strongly bind CO is a crucial factor for defining its activity towards CO_2 hydrogenation.[114]

Concerning the nature of the metal in the active sites, the better activity of the C-C coupling reaction (i.e., for C_2H_2 or CH_3CH_2OH generation) on Fe_5NC compared to Co_5NC has been attributed to the bigger discrepancy of the d electrons of the two CO-adsorbing Fe atoms.[114] A more general conclusion reported that M-N-C materials, with discrete and narrow metal d-states on their ACs, could be active CO_2RR catalysts, under the condition that HER is not competitive.[90] In addition to the optimum BE of CO_2RR intermediates, the electronic structure of the AC can also affect the selectivity of the M-N-C materials. For example, the better CO selectivity on Ni-N-C compared to Cu-N-C is explained by the electronic structure of the Cu-N_x sites, which, under cathodic conditions, the d-orbital of $Cu/Cu^{1+}/Cu^{2+}$ is filled by 9 or 10 electrons. This condition leads to the poor chemical stability of the Cu-N_x sites as the Cu-N coordination covalent bonds are compromised.[96] The selectivity of the M-N-C materials can also be affected by the coordination environment of metal at the AC.[88] In this context, DFT calculations demonstrated that the Ni-N_4 site is more selective for CO generation over HER compared to Ni-N.

Final remarks on CO_2RR

The present discussion makes clear that the nature of the metal centre in the M-N_x active sites plays a crucial role in defining the activity for the CO_2RR. Among the reviewed M-N-C (M=Fe, Co, or Ni) materials, Ni-N-C and Fe-N-C materials have hitherto been the most promising catalysts for CO_2RR. Regarding CO_2RR selectivity, the M-N-C catalysts highly favour CO production due to the moderate binding of CO_2RR intermediates at the M-N_x active sites. Furthermore, a variety of strategies have been reported to improve the selectivity and activity of CO_2RR on M-N-C catalysts. To mention a few these are: modulation of metal's

coordination environment, control of nitrogen functionalities, the introduction of dopants, and surface modification (e.g., nanoconfined ILs) are among the strategies that led to substantial enhancement of the electrocatalytic activity of M-N-C materials for this reaction. Regarding the stability during CO_2RR, so far, the stability time of these materials spans at maximum hundreds of hours, which, unfortunately, does not suffice the stability target of several thousands of hours for industrial CO_2 electrolysers.[85] The reasons for the deactivation of M-N-C catalysts after such operation times still lack a fundamental understanding of the degradation mechanism of M-N-C materials during CO_2RR. Comprehension of the deactivation process may only be accomplished after additional studies involving other better designed catalysts.

4. M-N-C (M=Fe, Co, or Ni) electrocatalysts for the HER

Although less frequent compared to ORR and CO_2RR, there are also works dealing with the investigation of M-N-C (M=Fe, Co, or Ni) catalysts for HER. Here we aim to describe the most promising strategies reported so far to enhance stability and HER activity on these types of materials.

In aqueous solutions, HER comprises three steps, as shown in Figure 14. The first step is the electrochemical reduction of hydronium (H_3O^+) or water (Volmer reaction), depending on the electrolyte pH, to produce adsorbed hydrogen atoms ($H_{(ads)}$). Following this, the adsorbed species react with another $H_{(ads)}$ that arises from the electrolytic H_3O^+/water reduction by the so-called Heyrovský reaction, and/or via the $H_{(ads)}$ combination through the Tafel reaction.[115,116]

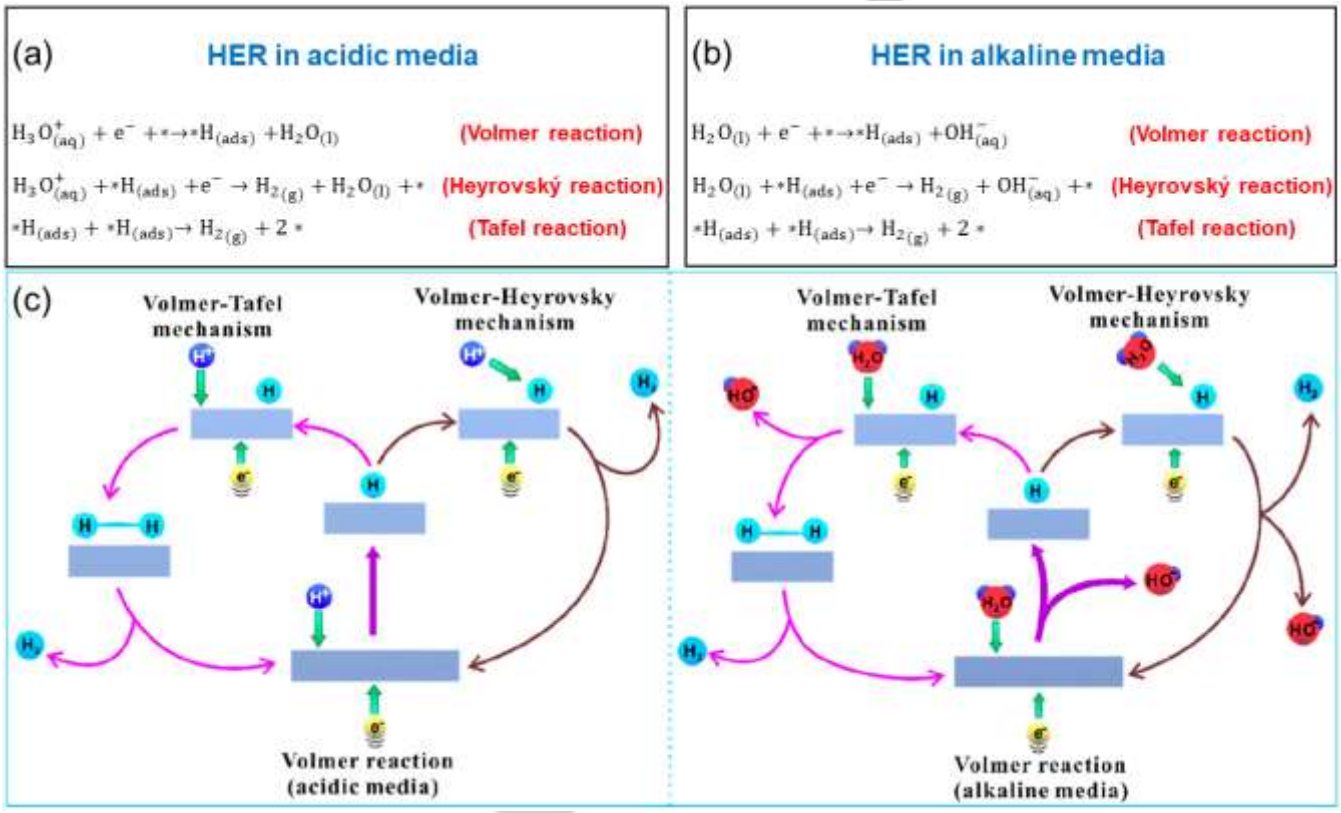

Figure 14. HER mechanisms in (a) acidic and (b) alkaline media.[117] (c) Schematic representation of HER mechanisms. Reprinted (adapted) with permission from Ref.[118] Copyright 2020, American Chemical Society.

M-N-C catalysts containing Co

Similar to the ORR and CO_2RR, the electrocatalytic performance of M-N-C materials for the HER relies heavily on the nature of the metal centre. Aiming to screen the most electrocatalytic M-N-C material for HER, a theoretical study systematically evaluated different transition metal elements in a SAC-based M-N-C structure, i.e., each metal was coordinated with four pyridinic nitrogen atoms embedded in a graphene sheet (see Figure 15a).[119] The theoretical results suggested that Co-N-C material is the most promising candidate for HER since the Gibbs free energy for hydrogen adsorption reaction (ΔG_{H^*}) on this catalyst was closer to zero (i.e., $\Delta G_{H^*} = 0.13$ eV), as compared to those of the other M-N-C materials (cf. Figure 15b). It was also learnt that the more adequate adsorption strength of hydrogen on Co-N-C is related to a more adequate energy level of the active valence Co $3d_{z^2}$ orbital together with the partial occupation of the antibonding orbitals (cf. Figure 15c).[119,120] For M-N-C (M = Fe, Co, or Ni) materials, this screening study revealed the following increasing trend of HER activity: Ni-N-C << Fe-N-C < Co-N-C. This trend was confirmed experimentally by the overpotential at a current density of −10 mA cm^{-2} for HER, which revealed a smaller value for Co-N-C (−230 mV vs. RHE) compared to Ni-N-C (−590 mV vs. RHE) in an acid medium (cf. Figure 15d).[119] Theoretical studies have also focused on assessing the N-based sites (Figure 15e), which could be active for HER. DFT calculations suggested that terminal graphitic-N and Co-N are the possible active sites, as observed

by the descriptor for HER activity, i.e., the ΔG_{H^*} values closer to zero (Figure 15f). In addition, the theoretical analyses indicated the occurrence of the Volmer-Heyrovský mechanism for the HER on these sites (Figure 15g).[121] As also shown in Figure 15g, the activation energy barrier for the Volmer step at the Co-N site is negligible, whereas for the graphitic-N site, it is 0.24 eV. Such results suggest that the electrochemical hydrogen adsorption reaction (Volmer step) is very fast at the Co-N site. Additionally, the activation energy barrier for the Heyrovský step was much higher at the graphitic-N site compared to the Co-N site, implying that Co-N is a more active site for HER.

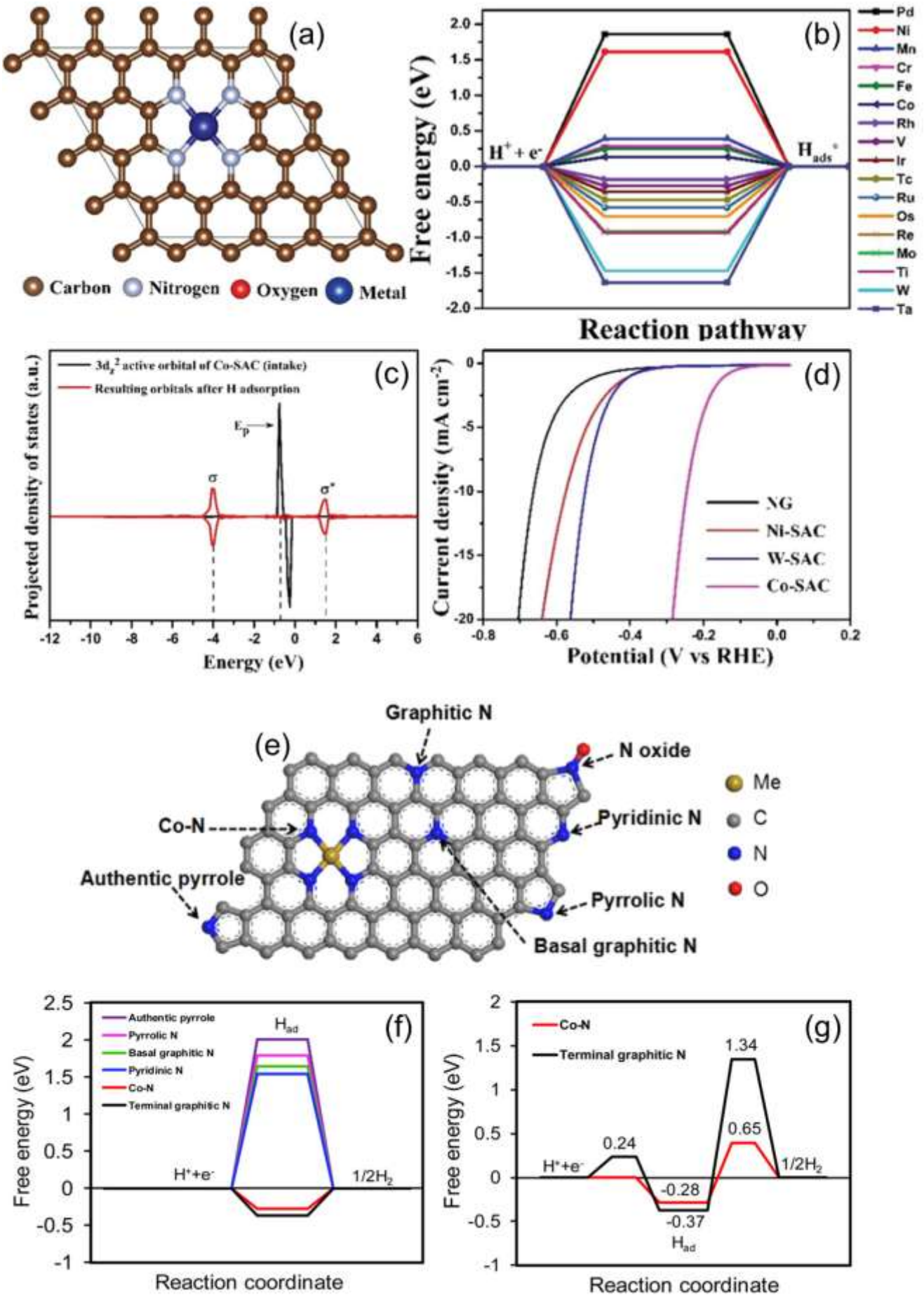

Figure 15. (a) SAC-based M-N-C model. (b) ΔG_{H^*} (Volmer reaction) for SAC-based M-N-C material with different transition metal elements. (c) Projected density of states for $3d_{z^2}$ active orbital (E_p, spin-up, and spin down) of SAC-based Co-N-C material which interacts with hydrogen and produces bonding (σ) and antibonding (σ*) orbitals. (d) Linear sweep voltammograms at a scan rate of 10 mV s^{-1} for SAC-based M-N-C (M=Ni, W, or Co) materials and the control sample (N-doped graphene (NG)) in 0.5 mol L^{-1} H_2SO_4. Reproduced (adapted) with permission.[119] Copyright 2019, Wiley. (e) N-based sites on a graphene sheet, (f) ΔG_{H^*} in a three-state-diagram for N-based sites, and (g) reaction barriers for Volmer-Heyrovský mechanism at the terminal graphitic-N and Co-N sites. Reprinted (adapted) with permission from Ref.[121] Copyright 2016, American Chemical Society.

Another promising strategy to improve (Co-N_4)-based catalysts is to modify the coordination environment of the metal centre by introducing other heteroatoms, e.g., phosphorus (i.e., Co-PN_3) via *in situ* phosphatisation. Compared to the Pt/C catalyst, this system delivered large HER activity and durability (for up to 15 h) in acidic medium, which was assigned to the increased length of the Co-N and Co-P bonds, and the high valence state of Co element in the Co-PN_3 moieties, as evidenced by combined DFT calculations and in situ XAS analyses.[122] Recently, a synthesis approach based on wet impregnation/pyrolysis was used to obtain Co-N-C featuring Co*-/N-C* bi-active sites supported on a hierarchical porous carbon structure,[123] and this system showed good performance and stability (up to 60 h) for HER in alkaline electrolyte. DFT calculations and in-situ Raman analyses indicated that positively charged Co nanoparticles in contact with the Co-N-C may have favoured water adsorption and activation, whilst the negatively charged carbon atoms next to N atoms could have accelerated the dissociation of $H_{(ads)}$-OH bonds in the Volmer-Heyrovský mechanism for the HER.

As mentioned previously, the typical pyrolysis step may lead to a heterogeneous distribution of sites in the M-N-C catalysts, which is deleterious to identify the active site responsible for promoting a particular electrocatalytic process. For Co-N-C material, such distribution may comprise of atomically dispersed Co-N_x sites and metallic Co nanoparticles encapsulated in graphitic carbon shells (Co@C).[124] Aiming to define the genuine active sites for the HER, Sa et al.[124] synthesised (see Figure 16a) a series of Co-N-C materials with controlled Co-N_x and Co@C site densities. On the basis of HER electrocatalytic performance, it was found that the Co-N_x sites, played a major role in the HER activity in both acidic and alkaline media, whereas the Co@C sites only exhibited minor catalytic effects. The contribution of the Co-N_x and Co@C sites for the HER activity was also assessed theoretically by DFT calculations. As shown in Figure 16b, the theoretical analyses indicated that CoN_4C_{10} model sites are the most plausible structure for promoting the HER as it results in near-thermoneutral H* adsorption energy (i.e., $\Delta G_{H^*} = -0.04$ eV). The Co@C sites were found to be very inactive for the HER regardless the nitrogen coordination type, as expected for obtained $\Delta G_{H^*} > 0.5$ eV (see Figure 16c). Regarding stability, the Co-N-C catalyst with Co-N_x sites exhibited a stability time up to 25 h in alkaline medium, which was superior to that of a Pt/C catalyst (see Figure 16d).

Besides optimisation of Co-N_x active site densities, it is also critical to note that industrial applications, such as commercial electrolysers, require catalysts that could reach *j* from 1 to 3 A cm^{-2}.[125] Aiming to attain such magnitudes of *j*, it has been recently reported the use of carbon film with vertically aligned microchannels (see the centre of Figure 16g) containing the SAC-based Co-N-C catalyst.[126] In terms of HER electrocatalytic performance, the Co-N-C catalyst exhibited outstanding *j* values of −500 and −1,000 mA cm^{-2} in acidic medium at overpotentials of −272 and −343 mV vs. RHE, respectively (cf. Figure 16e). Additionally, this material operated uninterruptedly and stably at −1,000 mA cm^{-2} for 32 h (see Figure 16f). Also, as summarised in Figure 16g, such improvements were assigned to combined effects of (i) high intrinsic activity of Co-N_x active sites; (ii) mass transfer facilitation by the aligned open microchannels and the multiscale porosity of the carbon; (iii) superhydrophilicity of the material; and (iv) fast detachment of H_2 bubbles due to superaerophobicity effects.

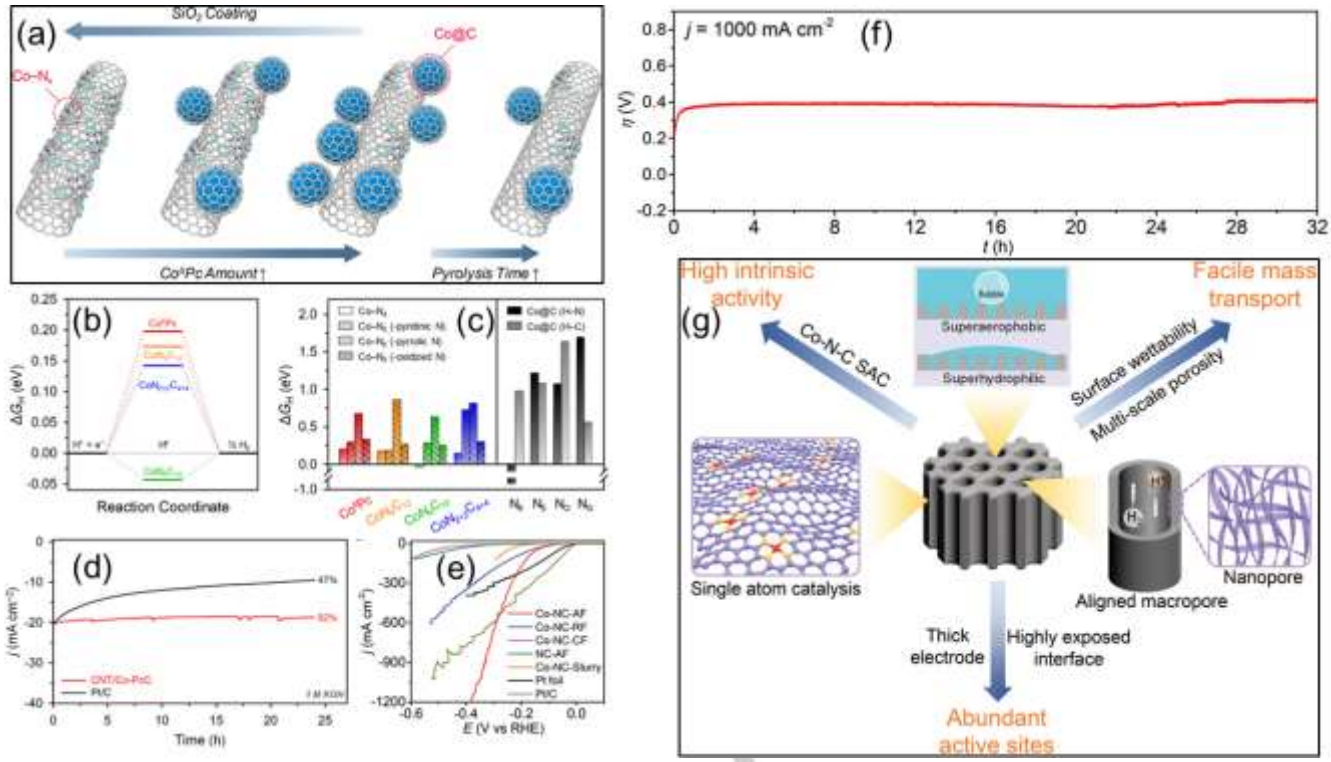

Figure 16. (a) Representation of synthesis approach of Co(II) phthalocyanine ($Co^{II}Pc$) on the surface of carbon nanotubes (CNT) with controlled Co-N_x and Co@C site densities. Blue and red spheres denote Co and N atoms, respectively. (b) ΔG_{H^*} diagram for Co-N-C clusters. (c) Comparison of calculated ΔG_{H^*} values for Co-N_x and Co@C sites. (d) Chronoamperometric curves for CNT/Co-Pc and Pt/C catalysts in 1 mol L^{-1} KOH. Reprinted (adapted) with permission from Ref.[124] Copyright 2019, American Chemical Society. (e) Linear sweep voltammograms at a scan rate of 5 mV s^{-1} for Co-N-C and Pt-based catalysts in 0.5 mol L^{-1} H_2SO_4. (f) Chronoamperometric curve at −1,000 mA cm^{-2}. (g) Design strategy of Co-N-C catalyst towards high *j* for HER. Reproduced (adapted) with permission.[126] Copyright 2021, Wiley.

M-N-C catalysts containing Fe

Many efforts have also been devoted to developing highly active Fe-N-C materials for HER. For example, it was achieved a good HER performance in alkaline medium for this material prepared via wet impregnation followed by pyrolysis.[127] In this study, Tafel slope analysis indicated the Volmer-Heyrovský mechanism for the HER, with the Heyrovský reaction being the RDS. In another study, Wang et al.[128] employed operando XAS to investigate a SAC-based Fe-N-C catalyst in alkaline media, which was previously characterised via the HAADF-STEM (Figure 17a-b). The K-edge XANES spectra (Figure 17c) indicated that the oxidation number is situated between +2 and +3 for the Fe atoms, while the L_3-edge XAS Fe spectra (Figure 17d) and the Fe-edge FT-EXAFS spectra (Figure 17e) demonstrated the presence of Fe-N coordination and absence of Fe-Fe bonds, thus indicating the presence of SAC-based structure for Fe-N-C catalyst. Based on EXAFS fitting analyses (Figure 17f), the authors also demonstrated that the coordination number was nearly four, suggesting that the Fe atom was atomically coordinated by nearly four nitrogen atoms of the N-C matrix. From studies involving operando analyses at different overpotentials, the authors reported that under these conditions the Fe-support interaction is weak and both the Fe-N coordination number and Fe oxidation state underwent a decrease of their values at the conditions of more negative overpotential values (Figure 17g-i). The occurrence of such structural modifications for the Fe-N-C catalyst was demonstrated to favour the HER in alkaline medium. Also from the electrochemical results, it was proposed the occurrence of the Volmer-Heyrovský pathway (Figure 17j) and water dissociation was the RDS for the HER on the SAC-based Fe-N_x active sites.

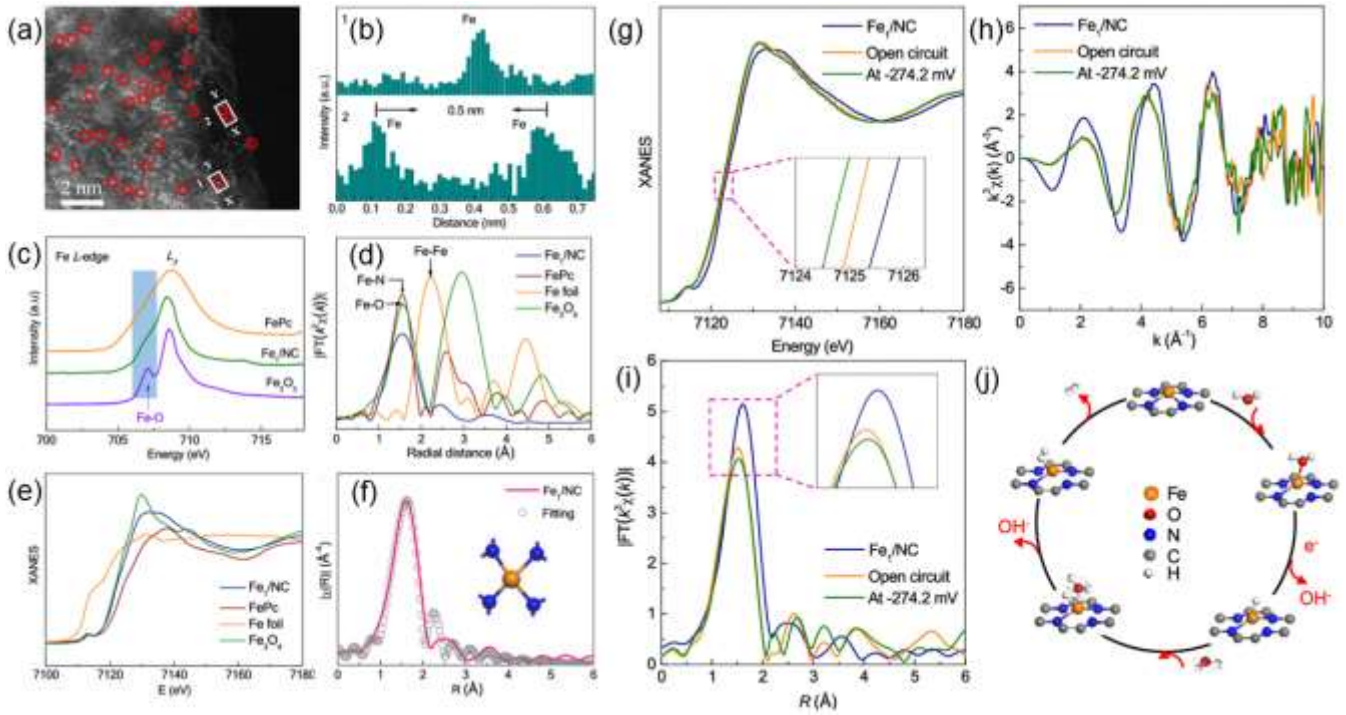

Figure 17. (a) HAADF-STEM image and (b) intensity profile along the lines X-Y in panel (a) for Fe-N-C catalyst. (c) XANES spectra at the Fe K-edge for Fe-N-C catalyst, Fe phthalocyanine (FePc), Fe foil, and Fe_3O_4. (d) Fe L_3-edge curves for Fe-N-C catalyst, FePc, and Fe_2O_3. (e) FT-EXAFS spectra at the Fe K-edge for Fe-N-C catalyst, FePc, Fe foil, and Fe_3O_4. (f) The R-space curve-fitting for Fe-N-C catalyst and the proposed Fe-N_4 configuration. (g) Operando XANES spectra at the Fe K-edge, (h) corresponding Re($k^3(\chi(k))$ and (i) k^3-weight FT-EXAFS curves for Fe-N-C catalyst. (j) Proposed HER mechanism on Fe-N-C catalyst in alkaline medium. All potentials are quoted with respect to the RHE. Reprinted (adapted) with permission from Ref.[128] Copyright 2020, American Chemical Society.

M-N-C catalysts containing Ni

The nitrogenation/exfoliation process has been employed to obtain chemically stable Ni-N-C nanosheets with thickness of <2 nm and this catalyst showed good catalytic activity for HER in a broad variety of pH.[129] For example, in acidic medium, this catalyst delivered an activity near to that of Pt/C catalyst, and also good stability (up to 70 h). Another illustrative study demonstrated that in alkaline media the HER activity is considerably high for Ni-N-C catalyst containing Ni-N_{2+2}-S active sites, anchored on a hierarchical porous carbon structure. Based on DFT calculations, it was shown that the introduction of sulphur atoms in the Ni-N_x sites (i.e., Ni-N_{2+2}-S) resulted in a substantial d-band centre upshift compared to the pristine Ni-N_4, and this led to a more stabilised OH adsorption. Additionally, the synergetic duas-site (Ni and S atoms) favoured a suitable adsorption strength of the intermediate species ($OH_{(ads)}$ and $H_{(ads)}$), which reflected in an improved water dissociation kinetics and high stability of the material (up to 25 h) in alkaline medium.[130]

Final remarks on HER

Albeit considerable advancements have been achieved over the years for HER on M-N-C catalysts, understanding the electrocatalytic properties of these materials for HER is still in the early stage. The stability of M-N-C materials also stands as a critical factor, as the M-N-C materials' stability time spans at maximum tens of hours, which, is considerably inferior to the 60,000-90,000 h required for practical water electrolysers.[131] Considering the nature of the metal centre, a screening study proposed the following trend of increasing HER activity: Ni-N-C << Fe-N-C < Co-N-C.[119] Additionally, the few studies regarding the HER mechanism seem to confirm that this reaction is composed of the Volmer and Heyrovský steps, being the latter the possible RDS. Also, the present understanding indicates that further efforts are required to optimise HER electrocatalysis and the long-term stability of M-N-C materials.

5. Summary

Compared to the conventional precious metal catalysts (i.e., platinum-group metals as well as Au and Ag metals), M-N-C (M=Fe, Co, or Ni) catalysts have reached a stage of good electrocatalytic activity and durability for ORR, CO_2RR, and HER, particularly the first two reactions. The nature of the metal centre in the M-N-C catalysts is proved to be critically important for the occurrence of a given electrochemical reduction reaction. Currently, Fe-N-C material is the most suitable candidate to substitute noble metal catalysts for ORR, whilst Ni-N-C often displays better performance than Fe-N-C and Co-N-C materials for CO_2-to-CO conversion. For the HER, the M-N-C catalysts have not yet reached satisfactory electrocatalytic performance. Nevertheless, Co-N-C stands as a possible candidate, for HER compared to Fe-N-C and Ni-N-C materials. Concerning the strategies that effectively enabled the improvement of electrocatalytic properties of the M-N-C materials, those related to modification of the surface and bulk regions via the introduction of ILs and dopants (mainly phosphorus and sulphur) seem to be most effective. Enlargement of specific-surface-area and increase

of active sites density, as well as control of the coordination environment have provided improvement of electrocatalytic performance. Efforts have also been spent to understand and mitigate the degradation process of M-N-C materials, yet further studies are still required. It is worth noting that bimetallic M-N-C systems as well as dopants bonded to the metal centre are considered promising strategies to minimise the demetallation process. Last but not least, theoretical knowledge on M-N-C materials is in the state of gathering momentum to become a viable tool for optimising and improving their application in electrocatalysis. So far, theoretical activity descriptors should be used carefully, as they could oversimplify highly complex processes. There is still a big gap in the theoretical understanding of the ORR, CO_2RR, and HER on M-N-C catalysts compared with other conventional catalysts.

6. Outlook

Examining how much we have learnt about M-N-C (M=Fe, Co, or Ni) materials towards ORR, CO_2RR, and HER, it comes apparent that enormous advances have been accomplished in terms of fundamental science thus far. But many questions remain unanswered and clarifying them is pivotal for practical applications. One of these questions concerns the typical synthetic routes to produce M-N-C materials which often lead to a poor number of metal atoms bonded to the nitrogen atoms, thus compromising the maximisation of M-N_x active sites density. Current works that produce M-N-C materials by pyrolysis often investigate the role of pyrolysis temperature on the textural, structural, and electrochemical performance. However, it is difficult to find studies to elucidate the impact of heating and cooling rates. Fast heating rates often result in high gas outflux, which can introduce defects in the M-N-C materials. Also, for Zn-N-C material, low heating rates effectively increased the metal site content in the material.[132] Thus, the heating rate for pyrolyzing M-N-C precursors seems to be an important factor and deserves to be carefully evaluated.

Finding novel strategies for improving catalytic activity and understanding the electronic structure of these materials may be a coherent way to envisage a rational synthesis route for M-N-C materials featuring better electrocatalytic performances. Additionally, modern characterisation methods can help researchers to elucidate the origins of the catalytic activity and their deactivation process. In situ and operando methods are powerful tools for correlating the electronic structure and electrochemical responses,[133–135] but this approach lacks studies for investigating the loss of catalytic activity. A promising procedure to investigate the nature of the deactivation process can be via the employment of advanced characterisation techniques, such as identical location high-resolution transmission electron microscopy. Such investigations are pivotal for proposing a rational design of stable catalysts.

In addition to the electrochemical measurements in a three-electrode setup, the evaluation of devices (i.e., two-electrode configuration), such as fuel cells, stands as an interesting approach to accessing the performance of M-N-C materials. For application in devices, regularly, porous carbon-based M-N-C materials are prone to pore flooding during operando conditions, and this is hypothesised as one of the degradation mechanisms due to the reduction of the number of active sites.[136] Tuning the surface with hydrophobic groups is a promising strategy for controlling water penetration.

In view of what has been presented, the development of alternative strategies to overcome the present challenges (especially stability) is the key to shifting the employment of M-N-C catalysts from laboratory scale to commercial devices.

Acknowledgements

We would like to acknowledge the following Brazilian research funding agencies for financial support: grant #2021/01268-3, #2019/22183-6, #2020/11947-2, #2021/14163-5 and #2020/15230-5 (FAPESP/SHELL), São Paulo Research Foundation (FAPESP); Fundação de Apoio à Universidade de São Paulo (FUSP); and Conselho Nacional de Desenvolvimento Científico e Tecnológico – CNPq (163342/2020-2).

Keywords: electrocatalysis • electrochemical carbon dioxide reduction • hydrogen • hydrogen evolution reaction • oxygen reduction reaction • density functional calculations

[1] L. Peng, Z. Wei, *Engineering* **2020**, *6*, 653–679.

[2] Z. Liang, H. Zheng, R. Cao, *Sustain. Energy Fuels.* **2020**, *4*, 3848–3870.

[3] A. G. Rajan, J. M. P. Martirez, E. A. Carter, *ACS Catal.* **2020**, *10*, 11177–11234.

[4] M. B. Costa, M. A. de Araújo, M. V. d. L. Tinoco, J. F. de Brito, L. H. Mascaro, *J. Energy Chem.* **2022**, *73*, 88–113.

[5] S. Fankhauser, S. M. Smith, M. Allen, K. Axelsson, T. Hale, C. Hepburn, J. M. Kendall, R. Khosla, J. Lezaun, E. Mitchell-Larson, M. Obersteiner, L. Rajamani, R. Rickaby, N. Seddon, T. Wetzer, *Nat. Clim. Chang.* **2022**, *12*, 15–21.

[6] S. Jin, Z. Hao, K. Zhang, Z. Yan, J. Chen, *Angew. Chemie - Int. Ed.* **2021**, *60*, 20627–20648.

[7] S. Li, X. Hao, A. Abudula, G. Guan, *J. Mater. Chem. A* **2019**, *7*, 18674–18707.

[8] H. Liu, Y. Zhu, J. Ma, Z. Zhang, W. Hu, *Adv. Funct. Mater.* **2020**, *30*, 1910534.

[9] H. Shen, T. Thomas, S. A. Rasaki, A. Saad, C. Hu, J. Wang, M. Yang, *Electrochem. Energy Rev.* **2019**, *2*, 252–276.

[10] A. B. Laursen, A. S. Varela, F. Dionigi, H. Fanchiu, C. Miller, O. L. Trinhammer, J. Rossmeisl, S. Dahl, *J. Chem. Educ.* **2012**, *89*, 1595–1599.

[11] P. Sabatier, *La Catalyse en Chimie Organique*, Librairie Polytechnique, CH. Béranger, Paris, France **1913**.

[12] H.-F. Wang, C. Tang, Q. Zhang, *Adv. Funct. Mater.* **2018**, *28*, 1803329.

[13] Q. Lu, J. Rosen, Y. Zhou, G. S. Hutchings, Y. C. Kimmel, J. G. Chen, F. Jiao, *Nat. Commun.* **2014**, *5*, 3242.

[14] A. Kumar, V. K. Vashistha, D. K. Das, S. Ibraheem, G. Yasin, R. Iqbal, T. A. Nguyen, R. K. Gupta, M. R. Islam, *Fuel* **2021**, *304*, 121420.

[15] R. Jasinski, *Nature* **1964**, *201*, 1212–1213.

[16] J.-P. Dodelet, in *N_4-Macrocyclic Metal Complexes* (Eds. J. H. Zagal, F. Bedioui, J.-P. Dodelet), Springer, New York, United States of America **2006**, Ch. 3.

[17] C. Jia, K. Dastafkan, C. Zhao, *Curr. Opin. Electrochem.* **2022**, *31*, 100854.

[18] T. Tang, L. Ding, Z. Jiang, J.-S. Hu, L.-J. Wan, *Sci. China Chem.* **2020**, *63*, 1517–1542.

[19] X. Liang, Z. Li, H. Xiao, T. Zhang, P. Xu, H. Zhang, Q. Gao, L. Zheng, *Chem. Mater.* **2021**, *33*, 5542–5554.

[20] A. Zitolo, V. Goellner, V. Armel, M.-T. Sougrati, T. Mineva, L. Stievano, E. Fonda, F. Jaouen, *Nat. Mater.* **2015**, *14*, 937–942.

[21] N. N. Greenwood, T. C. Gibb, *Mössbauer Spectroscopy*, Chapman and Hall Ltd, London, UK **1971**.

[22] S. Gupta, D. Tryk, I. Bae, W. Aldred, E. Yeager, *J. Appl. Electrochem.* **1989**, *19*, 19–27.

[23] U. A. do Rêgo, T. Lopes, J. L. Bott-Neto, A. A. Tanaka, E. A. Ticianelli, *J. Electroanal. Chem.* **2018**, *810*, 222–231.

[24] U. A. do Rêgo, T. Lopes, J. L. Bott-Neto, A. M. Gómez-Marin, A. A. Tanaka, E. A. Ticianelli, *Electrocatalysis* **2019**, *10*, 134–148.

[25] K. Zhang, W. Guo, Z. Liang, R. Zou, *Sci. China Chem.* **2019**, *62*, 417–429.

[26] U. A. do Rêgo, R. Sgarbi, T. Lopes, C. C. dos Santos, A. A. Tanaka, E. A. Ticianelli, *Electrocatalysis* **2021**, *12*, 548–563.

[27] F. Luo, C. H. Choi, M. J. M. Primbs, W. Ju, S. Li, N. D. Leonard, A. Thomas, F. Jaouen, P. Strasser, *ACS Catal.* **2019**, *9*, 4841–4852.

[28] S. S. Kocha, K. Shinozaki, J. W. Zack, D. J. Myers, N. N. Kariuki, T. Nowicki, V. Stamenkovic, Y. Kang, D. Li, D. Papageorgopoulos, *Electrocatalysis* **2017**, *8*, 366–374.

[29] H. Xu, D. Wang, P. Yang, A. Liu, R. Li, Y. Li, L. Xiao, J. Zhang, M. An, *Phys. Chem. Chem. Phys.* **2020**, *22*, 28297–28303.

[30] K. Y. Vinogradov, A. V. Bulanova, R. V. Shafigulin, E. O. Tokranova, A. M. Mebel, H. Zhu, *ACS Omega* **2022**, *7*, 7066–7073.

[31] X. Yang, Y. Zeng, W. Alnoush, Y. Hou, D. Higgins, G. Wu, *Adv. Mater.* **2022**, *34*, 2107954.

[32] J. An, Y. Feng, Q. Zhao, X. Wang, J. Liu, N. Li, *Environ. Sci. Ecotechnology* **2022**, *11*, 100170.

[33] Y. Sun, L. Silvioli, N. R. Sahraie, W. Ju, J. Li, A. Zitolo, S. Li, A. Bagger, L. Arnarson, X. Wang, T. Moeller, D. Bernsmeier, J. Rossmeisl, F. Jaouen, P. Strasser, *J. Am. Chem. Soc.* **2019**, *141*, 12372–12381.

[34] W. Wang, Q. Jia, S. Mukerjee, S. Chen, *ACS Catal.* **2019**, *9*, 10126–10141.

[35] R. Sgarbi, K. Kumar, F. Jaouen, A. Zitolo, E. A. Ticianelli, F. Maillard, *J. Solid State Electrochem.* **2021**, *25*, 45–56.

[36] X. Yan, C. Fu, C. Lin, H. Hu, S. Shen, G. Wei, J. Zhang, *Prog. Nat. Sci. Mater. Int.* **2020**, *30*, 896–904.

[37] D. Wu, W. Liu, J. Hu, C. Zhu, H. Jing, J. Zhang, C. Hao, Y. Shi, *Mater. Chem. Front.* **2021**, *5*, 3093–3098.

[38] J. Müller-Hülstede, D. Schonvogel, H. Schmies, P. Wagner, A. Dyck, M. Wark, *ACS Appl. Energy Mater.* **2021**, *4*, 6912–6922.

[39] Q. Ma, H. Jin, J. Zhu, Z. Li, H. Xu, B. Liu, Z. Zhang, J. Ma, S. Mu, *Adv. Sci.* **2021**, *8*, 2102209.

[40] X. Luo, X. Wei, H. Wang, W. Gu, T. Kaneko, Y. Yoshida, X. Zhao, C. Zhu, *Nano-Micro Lett.* **2020**, *12*, 163.

[41] Y. Li, X. Liu, L. Zheng, J. Shang, X. Wan, R. Hu, X. Guo, S. Hong, J. Shui, *J. Mater. Chem. A* **2019**, *7*, 26147–26153.

[42] D. Xia, X. Tang, S. Dai, R. Ge, A. Rykov, J. Wang, T.-H. Huang, K.-W. Wang, Y. Wei, K. Zhang, J. Li, L. Gan, F. Kang, *Adv. Mater.* **2023**, *35*, 2204474.

[43] Q. Jia, N. Ramaswamy, H. Hafiz, U. Tylus, K. Strickland, G. Wu, B. Barbiellini, A. Bansil, E. F. Holby, P. Zelenay, S. Mukerjee, *ACS Nano* **2015**, *9*, 12496–12505.

[44] L. Li, Y. Wen, G. Han, Y. Liu, Y. Song, W. Zhang, J. Sun, L. Du, F. Kong, Y. Ma, Y. Gao, J. Wang, C. Du, G. Yin, *Chem. Eng. J.* **2022**, *437*, 135320.

[45] T. Marshall-Roth, N. J. Libretto, A. T. Wrobel, K. J. Anderton, M. L. Pegis, N. D. Ricke, T. V. Voorhis, J. T. Miller, Y. Surendranath, *Nat. Commun.* **2020**, *11*, 5283.

[46] C. Maouche, J. Yang, S. H. Al-Hilfi, X. Tao, Y. Zhou, *ACS Appl. Nano Mater.* **2022**, *5*, 4397–4405.

[47] X. Qu, Y. Li, G. Li, R. Ji, S. Yin, X. Cheng, C. Wang, J. Yang, Y. Jiang, S. Sun, *Electrochim. Acta* **2022**, *403*, 139604.

[48] T. Mineva, I. Matanovic, P. Atanassov, M.-T. Sougrati, L. Stievano, M. Clémancey, A. Kochem, J.-M. Latour, F. Jaouen, *ACS Catal.* **2019**, *9*, 9359–9371.

[49] F. Wang, Y. Zhou, S. Lin, L. Yang, Z. Hu, D. Xie, *Nano Energy* **2020**, *78*, 105128.

[50] F. Kong, X. Cui, Y. Huang, H. Yao, Y. Chen, H. Tian, G. Meng, C. Chen, Z. Chang, J. Shi, *Angew. Chemie Int. Ed.* **2022**, *61*, e202116290.

[51] C. H. Choi, C. Baldizzone, G. Polymeros, E. Pizzutilo, O. Kasian, A. K. Schuppert, N. R. Sahraie, M.-T. Sougrati, K. J. J. Mayrhofer, F. Jaouen, *ACS Catal.* **2016**, *6*, 3136–3146.

[52] Q. Liu, S. Cao, Y. Qiu, L. Zhao, *Mater. Sci. Eng. B* **2017**, *223*, 159–166.

[53] J. Liu, C. Fan, G. Liu, L. Jiang, *Appl. Surf. Sci.* **2021**, *538*, 148017.

[54] A. Babuponnusami, K. Muthukumar, *J. Environ. Chem. Eng.* **2014**, *2* 557–572.

[55] R. Sgarbi, K. Kumar, V. A. Saveleva, L. Dubau, R. Chattot, V. Martin, M. Mermoux, P. Bordet, P. Glatzel, E. A. Ticianelli, F. Jaouen, F. Maillard, *Appl. Catal. B Environ.* **2022**, *311*, 121366.

[56] L. Bai, J. Liu, C. Jin, J. Zhang, F. Wang, *J. Mater. Chem. A* **2020**, *8*, 18767–18777.

[57] Y. He, Y. Jia, B. Yu, Y. Wang, H. Li, Y. Liu, Q. Tan, *Small* **2023**, *19*, 2206478.

[58] K. Wang, X. Zhang, X. Xiang, Y. Wang, D. Lyu, S. Xi, Z. Q. Tian, *ACS Appl. Mater. Interfaces* **2022**, *14*, 46548–46561.

[59] C. Maouche, Y. Wang, C. Cheng, W. Wang, Y. Li, W. A. Qureshi, P. Huang, A. Amjad, Y. Zhou, J. Yang, *J. Colloid Interface Sci.* **2022**, *623*, 146–154.

[60] L. Fan, X. Wei, X. Li, Z. Liu, M. Li, S. Liu, Z. Kang, F. Dai, X. Lu, D. Sun, *Nano Res.* **2023**, *16*, 1810-1819.

[61] H. Han, X. Wang, X. Zhang, *J. Colloid Interface Sci.* **2022**, *615*, 617–626.

[62] M. Fang, G. Dong, R. Wei, J. C. Ho, *Adv. Energy Mater.* **2017**, *7*, 1700559.

[63] W. Wu, M. Wang, H. Huang, W. Gu, C. Yan, G. Chen, D. Yin, H. Jin, J. Wang, S. Wang, *J. Electron. Mater.* **2021**, *50*, 3078–3083.

[64] Y. Chen, Z. Li, Y. Zhu, D. Sun, X. Liu, L. Xu, Y. Tang, *Adv. Mater.* **2019**, *31*, 1806312.

[65] M. Rauf, J. Wang, S. Handschuh-Wang, Z. Zhou, W. Iqbal, S. A. Khan, L. Zhuang, X. Ren, Y. Li, S. Sun, *Prog. Nat. Sci. Mater. Int.* **2022**, *32*, 27–33.

[66] H. Adabi, A. Shakouri, N. U. Hassan, J. R. Varcoe, B. Zulevi, A. Serov, J. R. Regalbuto, W. E. Mustain, *Nat. Energy* **2021**, *6*, 834–843.

[67] Y.-P. Ku, K. Ehelebe, A. Hutzler, M. Bierling, T. Böhm, A. Zitolo, M.

Vorokhta, N. Bibent, F. D. Speck, D. Seeberger, I. Khalakhan, K. J. J. Mayrhofer, S. Thiele, F. Jaouen, S. Cherevko, *J. Am. Chem. Soc.* **2022**, *144*, 9753–9763.

[68] H. Tian, A. Song, P. Zhang, K. Sun, J. Wang, B. Sun, Q. Fan, G. Shao, C. Chen, H. Liu, Y. Li, G. Wang, *Adv. Mater.*, DOI: 10.1002/adma.202210714.

[69] X. Wang, H. Zhu, C. Yang, J. Lu, L. Zheng, H.-P. Liang, *Carbon* **2022**, *191*, 393–402.

[70] H. Xu, L. Xiao, P. Yang, X. Lu, L. Liu, D. Wang, J. Zhang, M. An, *J. Colloid Interface Sci.* **2023**, *638*, 242–251.

[71] M. Liu, L. Wang, L. Zhang, Y. Zhao, K. Chen, Y. Li, X. Yang, L. Zhao, S. Sun, J. Zhang, *Small* **2022**, *18*, 2104934.

[72] X. Xie, C. He, B. Li, Y. He, D. A. Cullen, E. C. Wegener, A. J. Kropf, U. Martinez, Y. Cheng, M. H. Engelhard, M. E. Bowden, M. Song, T. Lemmon, X. S. Li, Z. Nie, J. Liu, D. J. Myers, P. Zelenay, G. Wang, G. Wu, V. Ramani, Y. Shao, *Nat. Catal.* **2020**, *3*, 1044–1054.

[73] X. X. Wang, V. Prabhakaran, Y. He, Y. Shao, G. Wu, *Adv. Mater.* **2019**, *31*, 1805126.

[74] T. Sun, B. Tian, J. Lu, C. Su, *J. Mater. Chem. A* **2017**, *5*, 18933–18950.

[75] J. Y. Jung, S. Kim, J.-G. Kim, M. J. Kim, K.-S. Lee, Y.-E. Sung, P. Kim, S. J. Yoo, H.-K. Lim, N. D. Kim, *Nano Energy* **2022**, *97*, 107206.

[76] L. Zhao, Z. Lan, W. Mo, J. Su, H. Liang, J. Yao, W. Yang, *Nanomaterials* **2021**, *11*, 3429.

[77] J. Zhang, D. Cao, H. Liu, F. Wang, L. Liang, C. Liu, Q. Hao, Y. Li, *ChemPhysChem.* **2022**, *23*, e202100692.

[78] T. Patniboon, H. A. Hansen, *ACS Catal.* **2021**, *11*, 13102–13118.

[79] J. Mao, P. Liu, J. Li, D. Liang, J. Yan, W. Song, *Adv. Mater. Interfaces* **2019**, *6*, 1901186.

[80] G. Luo, Y. Wang, Y. Li, *Sci. Bull.* **2017**, *62*, 1337–1343.

[81] H. Xu, D. Cheng, D. Cao, X. C. Zeng, *Nat. Catal.* **2018**, *1*, 339–348.

[82] K. Liu, J. Fu, Y. Lin, T. Luo, G. Ni, H. Li, Z. Lin, M. Liu, *Nat. Commun.* **2022**, *13*, 2075.

[83] Y. Zheng, D.-S. Yang, J. M. Kweun, C. Li, K. Tan, F. Kong, C. Liang, Y. J. Chabal, Y. Y. Kim, M. Cho, J.-S. Yu, K. Cho, *Nano Energy* **2016**, *30*, 443–449.

[84] Z. Hao, Y. Ma, Y. Chen, P. Fu, P. Wang, *Nanomaterials* **2022**, *12*, 3331.

[85] I. E. L. Stephens, K. Chan, A. Bagger, S. W. Boettcher, J. Bonin, E. Boutin, A. K. Buckley, R. Buonsanti, E. R. Cave, X. Chang, S. W. Chee, A. H. M. da Silva, P. de Luna, O. Einsle, B. Endrődi, M. Escudero-Escribano, J. V. F. de Araujo, M. C. Figueiredo, C. Hahn, K. U. Hansen, S. Haussener, S. Hunegnaw, Z. Huo, Y. J. Hwang, C. Janáky, B. S. Jayathilake, F. Jiao, Z. P. Jovanov, P. Karimi, M. T. M. Koper, K. P. Kuhl, W. H. Lee, Z. Liang, X. Liu, S. Ma, M. Ma, H.-S. Oh, M. Robert, B. R. Cuenya, J. Rossmeisl, C. Roy, M. P. Ryan, E. H. Sargent, P. Sebastián-Pascual, B. Seger, L. Steier, P. Strasser, A. S. Varela, R. E. Vos, X. Wang, B. Xu, H. Yadegari, Y. Zhou, *J. Phys. Energy* **2022**, *4*, 042003.

[86] J. Li, P. Pršlja, T. Shinagawa, A. J. M. Fernández, F. Krumeich, K. Artyushkova, P. Atanassov, A. Zitolo, Y. Zhou, R. García-Muelas, N. López, J. Pérez-Ramírez, F. Jaouen, *ACS Catal.* **2019**, *9*, 10426–10439.

[87] S. Vijay, J. A. Gauthier, H. H. Heenen, V. J. Bukas, H. H. Kristoffersen, K. Chan, *ACS Catal.* **2020**, *10*, 7826–7835.

[88] C. Guo, T. Zhang, X. Liang, X. Deng, W. Guo, Z. Wang, X. Lu, C.-M. L. Wu, *Appl. Surf. Sci.* **2020**, *533*, 147466.

[89] Z. Zhang, L. Guo, Y. Han, L. Jiao, *Electrocatalysis* **2021**, *12*, 390–402.

[90] S. Vijay, W. Ju, S. Brückner, S.-C. Tsang, P. Strasser, K. Chan, *Nat. Catal.* **2021**, *4*, 1024–1031.

[91] S. Liang, L. Huang, Y. Gao, Q. Wang, B. Liu, *Adv. Sci.* **2021**, *8*, 2102886.

[92] R. Daiyan, X. Zhu, Z. Tong, L. Gong, A. Razmjou, R.-S. Liu, Z. Xia, X. Lu, L. Dai, R. Amal, *Nano Energy* **2020**, *78*, 105213.

[93] J. Tuo, Y. Lin, Y. Zhu, H. Jiang, Y. Li, L. Cheng, R. Pang, J. Shen, L. Song, C. Li, *Appl. Catal. B Environ.* **2020**, *272*, 118960.

[94] Y. Wang, L. You, K. Zhou, *Chem. Sci.* **2021**, *12*, 14065–14073.

[95] C. Wang, Y. Liu, H. Ren, Q. Guan, S. Chou, W. Li, *ACS Catal.* **2022**, *12*, 2513–2521.

[96] A. S. Varela, W. Ju, A. Bagger, P. Franco, J. Rossmeisl, P. Strasser, *ACS Catal.* **2019**, *9*, 7270–7284.

[97] C. Jia, X. Tan, Y. Zhao, W. Ren, Y. Li, Z. Su, S. C. Smith, C. Zhao, *Angew. Chemie Int. Ed.* **2021**, *60*, 23342–23348.

[98] F. Pan, B. Li, E. Sarnello, S. Hwang, Y. Gang, X. Feng, X. Xiang, N. M. Adli, T. Li, D. Su, G. Wu, G. Wang, Y. Li, *Nano Energy* **2020**, *68*, 104384.

[99] S. Lu, Y. Zhang, M. F. Mady, O. E. Eleri, W. M. Tucho, M. Mazur, A. Li, F. Lou, M. Gu, Z. Yu, *ChemSusChem* **2022**, *15*, e202200870.

[100] K. Li, S. Zhang, X. Zhang, S. Liu, H. Jiang, T. Jiang, C. Shen, Y. Yu, W. Chen, *Nano Lett.* **2022**, *22*, 1557–1565.

[101] X.-M. Hu, H. H. Hval, E. T. Bjerglund, K. J. Dalgaard, M. R. Madsen, M.-M. Pohl, E. Welter, P. Lamagni, K. B. Buhl, M. Bremholm, M. Beller, S. U. Pedersen, T. Skrydstrup, K. Daasbjerg, *ACS Catal.* **2018**, *8*, 6255–6264.

[102] Q. Sun, Y. Zhao, W. Ren, C. Zhao, *Appl. Catal. B Environ.* **2022**, *304*, 120963.

[103] X. Wang, X. Sang, C.-L. Dong, S. Yao, L. Shuai, J. Lu, B. Yang, Z. Li, L. Lei, M. Qiu, L. Dai, Y. Hou, Angew. Chemie Int. Ed. **2021**, *60*, 11959–11965.

[104] W. Ju, A. Bagger, X. Wang, Y. Tsai, F. Luo, T. Möller, H. Wang, J. Rossmeisl, A. S. Varela, P. Strasser, *ACS Energy Lett.* **2019**, *4*, 1663–1671.

[105] A. S. Varela, M. Kroschel, N. D. Leonard, W. Ju, J. Steinberg, A. Bagger, J. Rossmeisl, P. Strasser, *ACS Energy Lett.* **2018**, *3*, 812–817.

[106] B. J. Park, Y. Wang, Y. Lee, K.-J. Noh, A. Cho, M. G. Jang, R. Huang, K.-S. Lee, J. W. Han, *Small* **2021**, *17*, 2103705.

[107] W. Zheng, F. Chen, Q. Zeng, Z. Li, B. Yang, L. Lei, Q. Zhang, F. He, X. Wu, Y. Hou, *Nano-Micro Lett.* **2020**, *12*, 108.

[108] H. Yang, Q. Lin, C. Zhang, X. Yu, Z. Cheng, G. Li, Q. Hu, X. Ren, Q. Zhang, J. Liu, C. He, *Nat. Commun.* **2020**, *11*, 593.

[109] X. Wang, S. Feng, W. Lu, Y. Zhao, S. Zheng, W. Zheng, X. Sang, L. Zheng, Y. Xie, Z. Li, B. Yang, L. Lei, S. Wang, Y. Hou, *Adv. Funct. Mater.* **2021**, *31*, 2104243.

[110] C. Wang, H. Ren, Z. Wang, Q. Guan, Y. Liu, W. Li, *Appl. Catal. B Environ.* **2022**, *304*, 120958.

[111] Z. Li, R. Wu, S. Xiao, Y. Yang, L. Lai, J. S. Chen, Y. Chen, *Chem. Eng. J.* **2022**, *430*, 132882.

[112] J. Chen, T. Wang, X. Wang, B. Yang, X. Sang, S. Zheng, S. Yao, Z. Li, Q. Zhang, L. Lei, J. Xu, L. Dai, Y. Hou, *Adv. Funct. Mater.* **2022**, *32*, 2110174.

[113] A. Bagger, W. Ju, A. S. Varela, P. Strasser, J. Rossmeisl, *Catal.*

Today **2017**, *288*, 74–78.

[114] Q. Xue, X. Qi, T. Yang, J. Jiang, Q. Zhou, C. Fu, N. Yang, *Nanomaterials* **2022**, *12*, 2239.

[115] L. Xiao, Z. Wang, J. Guan, Coord. *Chem. Rev.* **2022**, *472*, 214777.

[116] J. Guan, X. Bai, T. Tang, *Nano Res.* **2022**, *15*, 818–837.

[117] K. J. Vetter, *Electrochemical Kinetics: Theoretical and Experimental Aspects*, Academic Press, New York, United States of America **1967**.

[118] J. Zhu, L. Hu, P. Zhao, L. Y. S. Lee, K.-Y. Wong, *Chem. Rev.* **2020**, *120*, 851–918.

[119] M. D. Hossain, Z. Liu, M. Zhuang, X. Yan, G.-L. Xu, C. A. Gadre, A. Tyagi, I. H. Abidi, C.-J. Sun, H. Wong, A. Guda, Y. Hao, X. Pan, K. Amine, Z. Luo, *Adv. Energy Mater.* **2019**, *9*, 1803689.

[120] D. Huang, Y. Luo, S. Li, L. Liao, Y. Li, H. Chen, J. Ye, *Mater. Horizons* **2020**, *7*, 970–986.

[121] L. Zhang, W. Liu, Y. Dou, Z. Du, M. Shao, *J. Phys. Chem. C* **2016**, *120*, 29047–29053

[122] J. Wan, Z. Zhao, H. Shang, B. Peng, W. Chen, J. Pei, L. Zheng, J. Dong, R. Cao, R. Sarangi, Z. Jiang, D. Zhou, Z. Zhuang, J. Zhang, D. Wang, Y. Li, *J. Am. Chem. Soc.* **2022**, *142*, 8431–8439.

[123] C.-F. Li, J.-W. Zhao, L. Xie, J.-Q. Wu, G.-R. Li, *Appl. Catal. B Environ.* **2021**, *282*, 119463.

[124] Y. J. Sa, S. O. Park, G. Y. Jung, T. J. Shin, H. Y. Jeong, S. K. Kwak, S. H. Joo, *ACS Catal.* **2019**, *9*, 83–97.

[125] J. K. Lee, C. Lee, K. F. Fahy, B. Zhao, J. M. LaManna, E. Baltic, D. L. Jacobson, D. S. Hussey, A. Bazylak, *Cell Reports Phys. Sci.* **2020**, *1*, 100147.

[126] R. Liu, Z. Gong, J. Liu, J. Dong, J. Liao, H. Liu, H. Huang, J. Liu, M. Yan, K. Huang, H. Gong, J. Zhu, C. Cui, G. Ye, H. Fei, *Adv. Mater.* **2021**, *33*, 2103533.

[127] W. d. S. Freitas, P. P. M. Pico, A. D'Epifanio, B. Mecheri, *Catalysts* **2021**, *11*, 1525.

[128] L. Wang, X. Liu, L. Cao, W. Zhang, T. Chen, Y. Lin, H. Wang, Y. Wang, T. Yao, *J. Phys. Chem. Lett.* **2020**, *11*, 6691–6696.

[129] J. Yin, Q. Fan, Y. Li, F. Cheng, P. Zhou, P. Xi, S. Sun, *J. Am. Chem. Soc.* **2016**, *138*, 14546–14549.

[130] J. Guo, W. Shang, J. Hu, C. Xin, X. Cheng, J. Wei, C. Zhu, W. Liu, Y. Shi, *ACS Appl. Mater. Interfaces* **2022**, *14*, 29822–29831.

[131] O. Schmidt, A. Gambhir, I. Staffell, A. Hawkes, J. Nelson, S. Few, *Int. J. Hydrogen Energy* **2017**, *42*, 30470–30492.

[132] J. Li, S. Chen, N. Yang, M. Deng, S. Ibraheem, J. Deng, J. Li, L. Li, Z. Wei, *Angew. Chemie Int. Ed.* **2019**, *58*, 7035–7039.

[133] L. Osmieri, R. K. Ahluwalia, X. Wang, H. T. Chung, X. Yin, A. J. Kropf, J. Park, D. A. Cullen, K. L. More, P. S. Zelenay, D. J. Myers, K. C. Neyerlin, *Appl. Catal. B Environ.* **2019**, *257*, 117929.

[134] K. Ebner, A. H. Clark, V. A. Saveleva, G. Smolentsev, J. Chen, L. Ni, J. Li, A. Zitolo, F. Jaouen, U. I. Kramm, T. J. Schmidt, J. Herranz, *Adv. Energy Mater.* **2022**, *12*, 2103699.

[135] J. Li, S. Ghoshal, W. Liang, M.-T. Sougrati, F. Jaouen, B. Halevi, S. McKinney, G. McCool, C. Ma, X. Yuan, Z.-F. Ma, S. Mukerjee, Q. Jia, *Energy Environ. Sci.* **2016**, *9*, 2418–2432.

[136] R. Peng, Z. Zhao, H. Sun, Y. Yang, T. Song, Y. Yang, J. Shao, H. Jin, H. Sun, Z. Zhao, *Chinese J. Chem.* **2023**, *41*, 710–724.

10.1002/cctc.202201594

WILEY-VCH

Entry for the Table of Contents

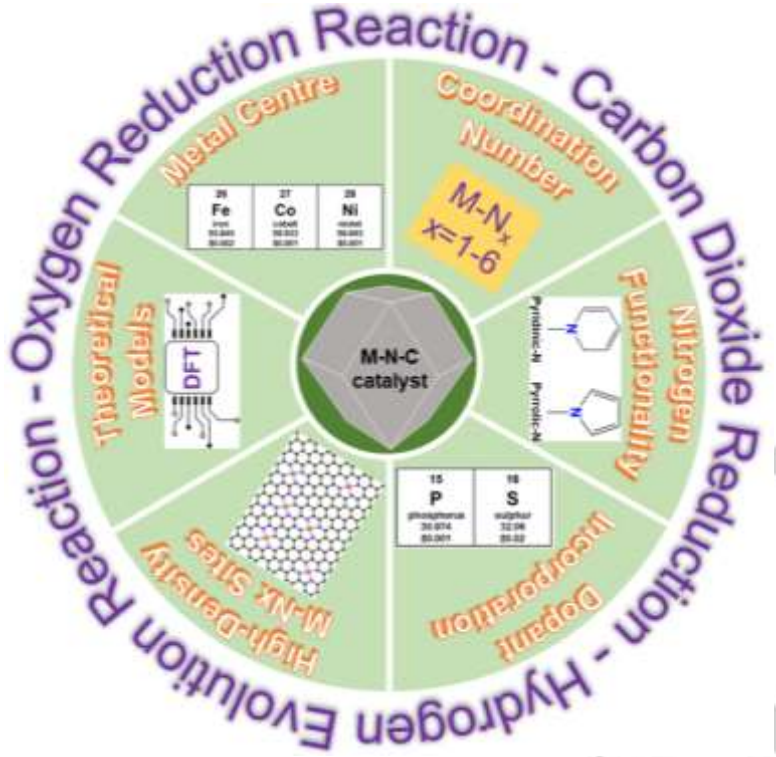

Strategies based on metal centre choice, introduction of dopants (e.g., phosphorus, and sulphur), coordination number control, modulation of nitrogen functionality, increase of M-N_x active sites density, and DFT-based theoretical models have recently been employed to further improve electrocatalytic performance and durability of M-N-C (M=Fe, Co, or Ni) catalysts for ORR, CO_2RR, and HER.

Researcher Twitter username: @AdeMoiss